NASA CR-132508

AN ANALYSIS OF THE IMPACT OF CABIN FLOOR ANGLE RESTRICTIONS ON L/D FOR A TYPICAL SUPERSONIC TRANSPORT

By R. L. Radkey

Prepared under Contract No. NAS1-13145 by

DOUGLAS AIRCRAFT COMPANY
MCDONNELL DOUGLAS CORPORATION
Long Beach, California

for

NATIONAL AERONAUTICS AND SPACE ADMINISTRATION

1. Report No.	2. Government Accession No.	3. Recipient's Catalog No.
NASA CR-132508		

4. Title and Subtitle	5. Report Date
An Analysis of the Impact of Cabin Floor Angle Restrictions on L/D for a Typical Supersonic Transport	August 1974
	6. Performing Organization Code
7. Author(s)	8. Performing Organization Report No.
R. L. Radkey	
	10. Work Unit No.
9. Performing Organization Name and Address	11. Contract or Grant No.
McDonnell Douglas Corporation Douglas Aircraft Company 3855 Lakewood Boulevard Long Beach, California 90846	NAS1-13145
	13. Type of Report and Period Covered
12. Sponsoring Agency Name and Address	Contractor Report
National Aeronautics and Space Administration Langley Research Center Hampton, Virginia 23665	14. Sponsoring Agency Code

15. Supplementary Notes

16. Abstract

High floor angles at cruise have been identified as a significant problem facing airline and public acceptance of a supersonic transport. In order to explore the relationship between cruise performance and floor angle, four related wing-fuselage design and integration studies have been conducted. The studies were:

1. A fuselage camber study in which perturbations in the fuselage camber distribution were examined with a baseline wing.

2. A wing optimization study in which wings were optimized for minimum drag at C_L's less than the design C_L. These wings were optimized as wing planform camber surfaces alone and evaluated with a baseline fuselage.

3. A second wing optimization study in which wings were optimized for minimum drag at C_L's less than the design C_L, but for this study the wings were optimized in the presence of the baseline fuselage.

4. A third wing optimization study in which wings were optimized for minimum drag subject to C_m constraints designed to produce more positive Cm_o's, thereby reducing trim drag.

The studies indicated that it was not possible to both improve the aircraft cruise L/D and substantially reduce the cruise floor angle. The studies did indicate that the cruise floor angle could be reduced by reducing the fuselage incidence relative to the wing, but the reduction in floor angle was accompanied by a substantial reduction in L/D.

17. Key Words (Suggested by Author(s))	18. Distribution Statement
Supersonic Transport, Configuration Optimization, Floor Angle	UNCLASSIFIED-UNLIMITED

19. Security Classif. (of this report)	20. Security Classif. (of this page)	21. No. of Pages	22. Price*
UNCLASSIFIED	UNCLASSIFIED	52	

* For sale by the National Technical Information Service, Springfield, Virginia 22151

AN ANALYSIS OF THE IMPACT OF CABIN FLOOR ANGLE RESTRICTIONS ON L/D FOR A TYPICAL SUPERSONIC TRANSPORT

By R. L. Radkey
Douglas Aircraft Company

SUMMARY

Four configuration design and integration studies have been conducted to determine whether a typical supersonic transport could be designed to achieve both high L/D's and low cabin floor angles at cruise. Numerous configuration perturbations about a baseline configuration were evaluated. The baseline configuration was designed for M = 2.2, C_L = 0.1, 273 passengers, and a maximum range of 7408 km (4000 n mi).

The first study, a fuselage camber study, was conducted to determine the effect of the fuselage camber distribution on the aircraft's cruise performance. It was concluded that fuselage camber variations fore and aft of the wing had little effect on L/D or the cruise floor angle. Low cabin floor angles were achieved by reducing the cabin floor incidence relative to the wing reference plane, but cruise L/D's were also significantly reduced.

The second study was a wing optimization study in which wings were optimized for minimum drag at C_L's less than the design C_L and then analyzed with the baseline fuselage. The study was conducted to determine whether wings requiring less incidence reduction near the root in order to be properly mated to the baseline fuselage might show better cruise performance. These wings had little effect on either cruise L/D or cruise floor angle.

The third study was a similar wing optimization study in which the wings were optimized in the presence of the baseline fuselage at C_L's less than the design C_L. It was found that L/D's could be increased up to 0.5 with approximately a 0.5 degree reduction in cruise floor angle.

The fourth study was a wing optimization study in which wings were optimized at the design C_L with pitching moment constraints designed to reduce the cruise trim drag. It was found that L/D could be increased up to 0.6 but the cruise floor angle was also increased nearly one degree.

The studies indicated that it was not possible to both improve the aircraft cruise L/D and substantially reduce the cruise floor angle below the five degrees of the baseline configuration. The studies did indicate that the cruise floor angle was reduced by reducing the fuselage incidence relative to the wing, but the reduction in cruise floor angle was accompanied by a substantial reduction in L/D.

INTRODUCTION

High floor angles at cruise have been identified as a significant problem facing airline and public acceptance of a supersonic transport. Configurations currently under study are anticipated to have cruise floor angles as high as seven degrees. The operators of current wide-bodied aircraft have already complained that cabin floor angles of two to three degrees add substantial difficulty and inconvenience to cabin operations. The carriers have expressed concern that floor angles as high as seven degrees may be virtually unacceptable in terms of cabin operations. In addition, the physical strain imposed on elderly passengers when moving about a high floor angle cabin may require an increase in cabin pressure and a corresponding increase in fuselage weight. The combination of these factors has resulted in a major problem which has not received adequate attention in the supersonic transport design process.

In order to explore the relationship between cruise performance and floor angle, four related wing-fuselage design and integration studies have been conducted. The studies evaluated numerous configuration perturbations about a baseline typical supersonic transport, the Douglas Aircraft Company D-3230-2.2-5. Recent detail design studies on the -5 configuration have built up a substantial data base which has made possible realistic, in-depth analyses not only of the aircraft's performance, but of the feasibility of integrating structurally the various wing-fuselage combinations under study. The studies conducted were:

1. A fuselage camber study in which perturbations in the fuselage camber distribution were examined with the baseline wing.

2. A wing optimization study in which wings were optimized for minimum drag at C_L's less than the design C_L. These wings were optimized as wing planform camber surfaces alone and evaluated with the baseline fuselage.

3. A second wing optimization study in which wings were again optimized for minimum drag at C_L's less than the design C_L, but this time the wings were optimized in the presence of the baseline fuselage.

4. A third wing optimization study in which wings were optimized for minimum drag subject to C_m constraints designed to produce more positive wing-body C_{m_o}'s. The more positive C_{m_o}'s have been found to reduce configuration trim drag.

CONFIGURATION ANALYSIS TECHNIQUES

Aerodynamic characteristics were determined by the Woodward Linearized Supersonic Analysis program (ref. 1). The Woodward program is a particularly useful design tool because of its versatility. It can be used to analyze wing camber surfaces, wing camber surfaces with thickness (thick wings), wing-body combinations and wing-body combinations with

external stores or axisymmetric nacelles. It can be used to optimize wings for minimum drag at a given C_L with or without a specified center of pressure, and it can be used to determine the wing shape corresponding to a given pressure distribution. It can be used to do either of the inverse problems in the presence of a body or stores. It can also be used to perform flow visualization by determining the flow properties at off-body points. The Woodward program uses a paneled interference cylinder to account for wing-body interference effects and gives reasonably accurate incremental differences between similar configurations. Program results have been shown to agree well with experimental data for numerous wing-body configurations.

All configurations were compared on the basis of trimmed aerodynamic performance as determined by a linearized trim drag program. Tail-off aerodynamic characteristics for the trim drag program were taken from Woodward wing-body runs. The zero-lift wave drag was determined by the Douglas Arbitrary Body Wave Drag program (refs. 2 and 3). The zero-lift wave drag was taken to be the same for all configurations because experience has shown that small changes in the wing and fuselage camber distributions had little effect on the wave drag. The skin friction drag was determined by using the turbulent flat plate with leading edge transition data from ref. 4. A form factor of 1.05 and a roughness factor of 1.06 were applied to the calculated skin friction drag. The friction drag was also taken to be the same for all configurations because the wetted area did not change significantly. Data used for the trim analysis on the baseline configuration are presented in Appendix A.

Downwash values at the tail for ϵ_o and $d\epsilon/d\alpha$ were determined by analyses of 2707-300 and SCAT 15 tail-on wind tunnel data. A downwash survey in the neighborhood of the horizontal tail was made with the Woodward flow visualization option in order to establish confidence in the experimental downwash values. The sensitivity of the trim drag program to accurate knowledge of the downwash was also investigated. The survey indicated that the experimental downwash values were acceptable for the -5 and that the study results would not have been appreciably effected by variations in the downwash of the magnitude observed in the survey. The downwash survey is discussed detail in Appendix B.

The English system of units (U. S. customary) was used as the principal system of measurement for this work.

SYMBOLS

AR	aspect ratio
b	reference wing span
C_D	drag coefficient, $\frac{\text{drag}}{q S_w}$
C_{D_f}	skin friction drag coefficient
C_{D_w}	zero-lift wave drag coefficient

C_L	lift coefficient, $\frac{\text{lift}}{q S_w}$
C_{L_A}	trimmed lift coefficient for the aircraft
C_m	pitching moment coefficient, $\frac{\text{moment}}{q S_w \bar{c}}$
C_{m_o}	zero-lift pitching moment coefficient
C_R	centerline root chord
D	drag
i_F	incidence of a floor section with respect to the wing reference plane (WRP)
i_w	incidence of any wing chord with respect to the WRP
L	lift
L/D	lift to drag ratio
M	Mach number
MAC	mean aerodynamic chord, $\bar{c}$
q	dynamic pressure, $1/2\ \rho V^2$
S_w	wing reference area
WRP	wing reference plane
X,Y,Z	stability axes with the wing reference plane defined as $Z = 0$
α	angle of attack, measured to the WRP
α_F	floor angle, measured from the WRP
α_o	zero-lift angle of attack
ϵ_o	downwash at zero angle of attack ($\alpha = 0$)
ϵ_α	downwash derivative, $d\epsilon/d\alpha$
η	nondimensional spanwise coordinate, $\frac{Y}{b/2}$
$(\ )_{wb}$	wing-body
$(\ )_t$	tail

BASELINE CONFIGURATION

The D-3230-2.2-5 configuration, shown in figure 1, was selected as the baseline configuration for the study because of the large volume of supporting data already availble. The -5 was designed according to accepted design procedures as pioneered by researchers at NASA's Langley Research Center. The methods set forth by Baals, Robins, and Harris (ref. 5) have consistently resulted in arrow wing configurations with good supersonic cruise performance as typified by the NASA SCAT 15 series of configurations. These configurations were designed by optimizing the wing for minimum drag at the cruise C_L and then laying the fuselage line of cross sectional area centroids along the wing root camber line. The fuselage cross sectional area distributions were selected by optimizing the fuselages for minimum zero-lift wave drag in the presence of the wing.

The -5 wing planform, W26, was selected by a wing planform comparison study conducted at M = 2.2, the design Mach number. W26 was then optimized for minimum drag at a C_L of 0.10 with no C_m constraints. The optimized wing incidence was 6^o at the most inboard wing defining section. This presented some difficulty in integrating the wing and fuselage because it had been decided that the cabin floor incidence with respect to the wing reference plane (WRP) would be restricted to 4^o in order to keep the floor angle at cruise reasonable. The floor angle at cruise was defined as the sum of the maximum floor incidence measured from the WRP plus the angle of attack measured to the WRP. In order to get the wing joined entirely beneath the cabin floor, the wing incidence at the most inboard defining section was reduced to 4^o. The incidence reduction was accomplished by rotating the most inboard defined wing section from 6^o incidence down to 4^o incidence. The inboard wing incidence distributions for the baseline and optimum wings are shown in figure 2. It can be seen that the actual wing incidence reduction at the wing-fuselage intersection was from 4.75^o to 3.60^o.

The -5 fuselage cross sectional area distribution was optimized for minimum wave drag subject to the constraints that there be adequate cockpit room and sufficient space for four-abreast seating. The component cross-sectional area build-up is shown in figure 3 for the -5 fuselage, wing, and tails. The minimum area for four-abreast seating and the sections where minimum areas were specified are also shown. The optimum area distribution was fitted to a cabin having flat floor segments with the wing segment oriented at 4^o incidence to the WRP. The resulting fuselage camber line came close to following the modified 4^o root camber (4RC) wing section.

Thus, the design procedure for the -5 departed slightly from the NASA procedure because of the restriction that the floor incidence be 4^o. For comparison, an "optimum" configuration with the -5 fuselage cross sectional area distributed along the 6^o optimum wing root was also analyzed.

The drag polars and C_m versus C_L curves for the baseline and optimum configurations are presented in figure 4. The untrimmed wing-body polars were quite similar for both configurations but the trim drag for the baseline configuration was substantially greater than for the optimum

configuration. The higher trim drag was directly the result of the larger nose down (negative) pitching moment developed by the baseline fuselage.

As $\partial C_m / \partial C_L)_{wing\text{-}body}$ was virtually the same for all configurations, the value of C_{m_o} was sufficient indication of the configuration pitching moment characteristics. In fact, C_{m_o} was an important indicator of configuration performance because the trim drag decreased as C_{m_o} became more positive.

Curves of L/D_{max} versus center of gravity location are shown in figure 5. It can be seen that the optimum configuration produced about 0.16 more in L/D_{max} at the nominal center of gravity location. This was directly attributable to the lower trim drag of the optimum configuration.

Curves of L/D versus floor angle for both configurations with center of gravity at its nominal location are shown in figure 6. The additional two degrees of floor incidence required to fit the fuselage along the optimum wing root camber line forced the cruise floor angle up to 7^o. In effect, the baseline configuration offered a 2^o reduction in floor angle at the expense of 0.16 in L/D.

Similar curves for farther aft center of gravity locations are shown in figure 7. These curves show that farther aft centers of gravity had little effect on the floor angle required for maximum L/D, but reduced the difference between L/D_{max} for the baseline and optimum configurations to about 0.10.

Curves of lift coefficient versus floor angle are presented for the trimmed aircraft in figure 8 indicating the C_{L_A} at which L/D_{max} occurred.

FUSELAGE CAMBER STUDY

The various fuselage camber distributions analyzed in the fuselage camber study are shown schematically in figure 9 and defined in detail in figure 10. The -5 fuselage camber was taken as the line of cross-sectional area centroids and was designated F-11. The two digits denoted the nose camber and tail camber used with the 4^o incidence center fuselage section to make up the camber line. The joggle in nose camber 1 was the result of cockpit visibility requirements. Tail camber 1 was upswept to meet rotation clearance criteria. Nose camber 2 and tail camber 2 were chosen to approximate axisymmetric sections aligned with the freestream. They were canted 1^o nosedown because the -5 baseline wing, W26-4RC, cruised at about 1^o angle of attack. The optimum fuselage camber line did not have to be canted because the optimum wing cruised at about 0^o angle of attack with angle of attack measured to the WRP. Nose camber 3 and tail camber 3 were configured solely to produce a more positive wing-body C_{m_o} by making the fuselage contribution more positive.

Each of the above fuselages was guaranteed a proper mating with the wing because the center sections followed the wing camber. But these variations tended to be ineffective in reducing the cruise floor angle, because the floor angle is the sum of the initial floor incidence and the angle of attack and the variations did not reduce the floor incidence which contributed 4° to the baseline configuration's cruise floor angle of 5°. So, a set of fuselage cambers representing flat floors set at less than 4° incidence to the WRP were also investigated. As the entire fuselage was rotated nose-down it was apparent that the wing would no longer lie entirely beneath the floor. It was readily apparent that the further the floor incidence was reduced, the more severe the weight penalties would be for having to run the wing carry-through structure around the cabin instead of under it.

Four low-incidence floor variations were studied. These were designated F-3.00D, F-1.92D, F-1.07D, and F-0.46D where the digits denoted the floor incidence in degrees. Structural weight penalties were anticipated to be severe as the floor incidence was reduced below 3.0° of incidence. It became nearly impossible to integrate the wing and fuselage when the wing reached the window line at 1.0° of floor incidence.

All fuselages analyzed had the same cross sectional area distribution as the baseline fuselage.

Effect of Nose Camber Variations

The effect of nose camber variations was studied by analyzing each of the three -5 nose variations with tail camber 2. Tail camber 2 was chosen because the fuselage camber aligned with the freestream fore and aft of the wing represents the supposed optimum configuration for that wing. Curves of L/D_{max} versus center of gravity location shown in figure 11 indicated that only nose camber 3, the upswept nose, showed any improvement. This was again directly attributable to a trim drag reduction due to a more positive C_{m_o}.

Curves of L/D versus floor angle are shown in figure 12 for the center of gravity at the nominal location. The nose camber variations showed only small L/D deviations from the baseline configuration.

The curves of trimmed aircraft lift coefficient, C_{L_A}, versus floor angle were virtually the same as for the baseline fuselage.

Effect of Tail Camber Variations

The effect of tail camber variations was studied by analyzing each of the tail variations with nose camber 2. Curves of L/D_{max} versus center of gravity location are presented in figure 13. Only tail camber 3, the upswept tail, showed any real improvement over the baseline. In this case however, the improvement was due to a reduction in wing-fuselage interference drag. The fuselage with the additional tail upsweep was sloped to take advantage of of the high pressure region on the underside of the aft fuselage caused by wing carry-over lift.

The curves of L/D versus floor angle shown in figure 14 reflected the 0.1 increase in L/D for tail camber 3, but showed no appreciable reduction in cruise floor angle at the L/D_{max} condition.

Just as for the nose camber variations, there was no change in the C_{L_A} versus floor angle relationship from the baseline configuration.

Effect of Combined Nose and Tail Camber Variations

The effect of combined nose and tail camber variations was determined by analyzing fuselage F-33 with the baseline wing and comparing it with the F-22 and baseline (F-11) configurations. Curves of L/D_{max} versus center of gravity location are shown in figure 15. Fuselage F-33 gave roughly the combined L/D_{max} increases of nose 3 and tail 3. The total improvement in L/D_{max} was only 0.1, however.

The L/D versus floor angle curves shown in figure 16 manifested almost no reduction in floor angle at the L/D_{max} condition.

The C_{L_A} versus floor angle curves showed no change from the baseline configuration.

Effect of Reduced Fuselage Incidence

Curves of L/D_{max} versus center of gravity location for the configurations with reduced floor incidence are presented in figure 17. The reductions evident in L/D_{max} resulted from increased drag-due-to-lift and trim drag. The increasingly negative C_{m_o}'s responsible for the additional trim drag resulted from a gradual reduction of the fuselage's contribution to the wing-body C_{m_o}.

The curves of L/D versus floor angle presented in figure 18 showed substantial reductions in cruise floor angle for configurations with decreased floor incidence. The accompanying penalties in L/D were, however, large, and they did not reflect the additional performance penalties, such as decreased range factor, due to increased structural weight.

Curves of C_{L_A} versus floor angle are shown in figure 19. The C_{L_A} for L/D_{max} was independent of the fuselage incidence angle.

WING OPTIMIZATION STUDY I - WINGS OPTIMIZED FOR MINIMUM DRAG AT C_L's LESS THAN THE DESIGN C_L

As stated earlier, wing planform 26 was originally optimized at $C_L = 0.1$ with no pitching moment constraint. The optimum wing incidence at the most inboard defining station was 6^o and had to be reduced to 4^o to ensure proper mating of the wing to the baseline fuselage. This incidence reduction caused

a drag-due-to-lift penalty which together with a trim drag penalty accounted for the difference between the baseline and optimum configurations. It was felt that a series of wings optimized alone (planform only) at C_L's less than 0.1 would require less incidence reduction near the root to meet the 4° fuselage floor constraint, thereby reducing the drag increase due to the incidence reduction.

For this study, wings were optimized at C_L's of 0.085, 0.070, 0.065, and 0.060. The incidence at the inboard defining section was exactly 4.0° for the wing optimized at $C_L = 0.065$. Where the inboard incidence was greater than 4°, it was reduced to 4°. The wings were then run with the baseline fuselage, fuselage F-11, to determine the wing-body aerodynamic characteristics for the trim drag analysis.

The inboard wing incidence distributions for the low C_L optimized wings are shown in figure 20. The wings were identified by their optimization C_L followed by a W which indicated the wings were optimized as planforms alone. The 4RC following the designation indicated that the inboard incidence was reduced to 4° from the optimum.

Curves of L/D_{max} versus center of gravity location are presented in figure 21. The low C_L optimized wings showed an L/D_{max} improvement of about 0.1 for the center of gravity at the nominal location, 24 percent MAC. In general, the wings showed better performance for the more forward center of gravity locations.

The curves of L/D versus floor angle shown in figure 22 indicated that the low C_L optimized wings cruised at higher floor angles than the baseline wing. They also showed that the 0.085W wing was the best of the series.

Curves of C_{L_A} versus nominal floor angle are shown in figure 23. The C_{L_A} for L/D_{max} decreased slightly for the wings optimized at lower C_L's.

WING OPTIMIZATION STUDY II - WINGS OPTIMIZED FOR MINIMUM DRAG AT C_L's LESS THAN THE DESIGN C_L IN THE PRESENCE OF A FUSELAGE

As pointed out earlier, the Woodward program can optimize wings in the presence of a fuselage. In this procedure, the wing portion of the configuration is optimized for minimum drag at a given C_L. Early attempts to optimize wing planform 26 in the presence of a fuselage were set aside because the optimum wing root incidence was in excess of 10°. In an attempt to circumvent this high root incidence problem, it was decided to optimize a series of wings in the presence of the baseline fuselage at C_L's less than the design C_L of 0.1.

For this study, wings were optimized at C_L's of 0.085, 0.070, 0.065 and 0.060 just as for the wing alone optimizations.

The inboard wing incidence distributions for wings optimized in the presence of the baseline fuselage are shown in figure 24. These wings were identified by their optimization C_L followed by a WB for wing-body optimization. The dashed lines in figure 24 indicate the root modification required to meet the 4° root camber constraint. The 0.060WB wing required no modification, the 0.070WB and 0.065WB wings required only a small amount of modification, but the 0.085WB wing presented a problem.

The 0.085WB-4RC wing was analyzed with the baseline fuselage, but some doubt had to be attached to the validity of the results. As shown in figure 24, the incidence at the wing-fuselage intersection was about 4.5°. When compared to 3.6° for the baseline fuselage, it was evident that the 0.085WB-4RC wing might not have fit under the 4° fuselage floor. In the absence of a detailed layout, only several observations could be made. First, if the wing could not have been fit under the floor, the wing gully inboard of $\eta = 0.12$ would have to have been emphasized. And second, it is doubtful that the Woodward program could have properly analyzed such a gully because the program is limited to approximately ten panels spanwise which should be of equal width for best results.

Curves of L/D_{max} versus center of gravity location are presented for the WB wings in figure 25. The wings showed improvement in L/D_{max} over a wide center of gravity range. This was due largely to a favorable trim drag situation in which the tail carried an upload rather than a download. The upload was required to trim the large positive C_m's generated by the wing-body optimized wings.

Curves of L/D versus floor angle are shown in figure 26 for the WB wings. The 0.085WB wing showed a reduction in cruise floor angle in addition to a substantial increase in L/D.

Curves of C_{L_A} versus floor angle are shown in figure 27. The C_{L_A} for L/D_{max} was slightly higher for the 0.085WB wing than for the baseline, but as seen for the wings optimized alone, C_{L_A} for L/D_{max} decreased as the optimization C_L decreased.

WING OPTIMIZATION STUDY III - WINGS OPTIMIZED FOR MINIMUM DRAG WITH C_m CONSTRAINTS

Wing 26 optimized at $C_L = 0.1$ with no C_m constraint yielded a wing-body C_{m_o} of -0.00114 when run with the baseline fuselage, F-11. The tail download required to trim this configuration produced trim drag equal to about three percent of the total aircraft drag at cruise. In an attempt to reduce the trim drag, a series of wings were optimized at $C_L = 0.1$ with C_m constraints designed to produce more positive C_{m_o}'s.

The wing optimized with no C_m constraint had a center of pressure located at 66 percent of the wing centerline root chord, C_R. To get more positive C_{m_o}'s the wings were optimized with the center of pressure

constrained to be at 62 percent C_R, 59 percent C_R, 56 percent C_R, and 53 percent C_R.

The inboard wing incidence distributions for the C_m constrained wings are shown in figure 28. In this study, the wings were identified by their specified center of pressure locations. The root incidence for these wings was considerably greater than for either set of wings optimized at C_L's less than the design C_L. The root camber modifications required to bring the incidence down to 4° were also more severe than for the low C_L wings.

The constrained wings achieved the desired change in center of pressure by redistributing the wing camber so that more load was carried farther forward. This change from the unconstrained optimum camber was accompanied by a degradation in drag-due-to-lift at the design C_L. Consequently, performance gains were a balance between reduced trim drag and increased drag-due-to-lift.

Curves of L/D_{max} versus center of gravity location for the C_m constrained wings are shown in figure 29. These curves showed the combined effects of trim drag benefits due to more positive C_{m_o}'s and drag decrements due to the nonoptimum wing warp. The trim drag benefits outweighed the wing drag-due-to-lift increases even for the 53 percent C_R wing. This can be seen by noting that L/D_{max} was still increasing for the 53 percent C_R constraint. For wings constrained farther forward, L/D_{max} would have fallen off because the drag-due-to-lift penalties would have become increasingly severe. These curves indicated that a wing constrained somewhere close to 53 percent C_R would have given the best overall aerodynamic performance at the nominal center of gravity location.

Curves of L/D versus floor angle are presented in figure 30 for the constrained wings. As the wings were constrained to farther forward centers of pressure, the floor angle for best L/D increased. For the 53 percent C_R wing, L/D_{max} occurred at almost 0.75° higher floor angle.

Curves of C_{L_A} versus floor angle are shown in figure 31. The C_{L_A} for L/D_{max} increased as the wings were increasingly constrained.

DISCUSSION

A comparison of L/D versus floor angle for the most promising configurations from each of the studies is presented in figure 32. The fuselage modification F-33 and the wing optimized alone at $C_L = 0.085$ each showed about 0.1 improvement in L/D at the nominal center of gravity location. While the wing alone optimization appeared unproductive in comparison to the other wing optimization procedures, the favorable effects of F-33 might easily be achieved on future configurations by upsweeping the tail. The nose camber 3 contribution to the L/D improvement shown by F-33 was small in comparison to the tail contribution, and it is unlikely that the nose camber upsweep will ever be implemented due to cockpit visibility requirements.

The configuration optimized at $C_L = 0.085$ in the presence of the baseline fuselage showed the most promise in terms of providing both a substantial increase in L/D, 0.45, and a reduction in cruise floor angle. The 53 percent C_R wing configuration showed the greatest improvement in L/D, 0.57, but at the cost of an additional degree in cruise floor angle.

The significance placed on these results depends on the importance attached to keeping the cruise floor angle low. Inasmuch as it does not appear possible to achieve cruise floor angles less than about 5 degrees and still obtain significant improvements in cruise L/D, it may be argued that the aircraft should be configured for maximum cruise efficiency and the high floor angles tolerated as a necessary evil. On the other hand, should it be decided that the floor angle must be held down to some arbitrary value, 3 degrees for instance, then a cruise L/D penalty must be expected. In this case a configuration with the floor at less than 4° incidence to the WRP appears worthy of exploration.

In general, the high floor angles of the well-performing configurations were the result of initially setting the floor incidence high so that the fuselage would not interrupt the wing lift distribution. Large floor angle reductions could only be achieved by reducing the floor incidence, and this meant reducing the fuselage incidence and disturbing the wing lift distribution.

It has been suggested that a saw-toothed or terraced floor could be used with a high incidence fuselage. This solution, however, introduces additional structural complexity which may result in a weight penalty and may require complicated duct and control line routing. The maneuvering of food carts over floor steps and the possible loss of seats due to cabin partitions are also objections to a terraced floor.

CONCLUSIONS

Four configuration perturbation studies have been conducted on a typical supersonic transport configuration designed for $M = 2.2$ and $C_L = 0.1$. Numerous fuselage and wing variations were examined to determine the impact of different configuration optimization techniques on cruise L/D and cruise floor angle. The following conclusions were drawn for the center of gravity nominally located at 24 percent MAC:

1. The baseline configuration was found to operate at an L/D_{max} of 9.34 with a cruise floor angle of 5.0°. This was only 0.16 less in L/D_{max} but a full 2.0° less in floor angle than for the optimum configuration.

2. Fuselage nose camber variations had very little effect on configuration performance or cruise floor angle.

3. The fuselage tail camber variation with two additional degrees of upsweep showed about 0.1 improvement in L/D_{max} and no change in cruise floor angle for the nominally located center of gravity. This configuration change appeared promising by virtue of the simplicity of implementing it.

4. Fuselage nose and tail camber variations showed approximately the combined improvement of the nose and tail variations taken separately. The 2^{o} upswept tail variation dominated the L/D improvement and there was no change in cruise floor angle.

5. Substantial cruise floor angle reductions were achieved by setting the fuselage at less than 4^{o} incidence with respect to the wing reference plane. The configurations did not appear to be structurally integrable for fuselage incidence angles below 1.0^{o}, and weight penalties were expected for fuselage incidence angles below 3.5^{o}. Unfortunately, substantial reductions in L/D_{max} accompanied the fuselage incidence reductions making these variations unattractive.

6. Wings optimized for minimum drag at C_L's less than the design C_L did not show any appreciable improvement in either L/D or cruise floor angle.

7. Wings optimized for minimum drag in the presence of the baseline fuselage at C_L's less than the design C_L showed substantial improvement in L/D and some reduction in cruise floor angle. The wing optimized at $C_L = 0.085$ showed the most promise with an L/D increase of 0.45 and a floor angle reduction of 0.5^{o}. The analysis of this configuration may have been inaccurate due to the formation of a gully near the wing root. The gully was required to mate the wing to the baseline fuselage and its three-dimensional nature may not have been adequately captured by the planar wing representation used in the analysis.

8. Wings optimized for minimum drag with C_m constraints designed to reduce cruise trim drag produced the greatest increases in L/D but also increased the cruise floor angle. The wing with center of pressure constrained to be at 53 percent of the centerline root chord, versus 66 percent for the unconstrained baseline wing, showed 0.57 improvement in L/D but was accompanied by a 0.75^{o} increase in the cruise floor angle.

It was not possible to both improve the aircraft cruise L/D and substantially reduce the cruise floor angle from the 5 degrees of the baseline configuration. In general, wing variations caused changes in L/D but did not effect the cruise floor angle more than a half degree. Small fuselage camber variations had little effect on L/D or cruise floor angle, and the large fuselage camber variations required to reduce the fuselage incidence brought the floor angle down but caused severe L/D penalties.

APPENDIX A

BASELINE CONFIGURATION DATA USED FOR TRIM DRAG ANALYSIS

Geometric characteristics		
Wing area	928 sq m	10,000 sq ft
Horizontal tail area	72.5 sq m	781 sq ft
Wing MAC, $\bar{c}$	19.8 m	64.9 ft
Tail MAC	7.04 m	23.0 ft
Tail aerodynamic center	1.762 $\bar{c}$ from the leading edge of the MAC	
Drag buildup data		
Zero-lift wave drag coefficient		0.00198
Skin friction drag coefficient including form and roughness factors		0.00435
Total lift independent drag coefficient		0.00633
Woodward tail-off aerodynamic characteristics		
Wing induced drag factor, K_w		0.5396
C_L for minimum induced drag, C_{L_o}		0.0191
Twist drag, $C_{D_{min}}$		0.00073
Wing-body aerodynamic center		26.78% MAC
Zero-lift pitching moment coefficient, C_{m_o}		-0.00114
Zero-lift angle of attack, α_o		-2.58^o
Wing-body lift curve slope, C_{L_α}		0.03233
Tail aerodynamic characteristics		
Tail induced drag factor, K_t		0.509
C_L for minimum induced drag $C_{L_{ot}}$		0.0
Tail twist drag, $C_{D_{min_t}}$		0.0
Tail zero-lift pitching moment coefficient, $C_{m_{ot}}$		0.0
Tail incidence, i_t		0.0
Tail lift curve slope, $C_{L_{\alpha_t}}$		0.025
Downwash		
Downwash at zero angle of attack, ϵ_o		1.0^o
$d\epsilon/d\alpha$		0.25

APPENDIX B

SENSITIVITY OF STUDY RESULTS TO ACCURATE KNOWLEDGE OF THE DOWNWASH

Because the downwash parameters ϵ_o and $d\epsilon/d\alpha$ were deduced from tail-on experimental data for the SCAT 15 and the 2707-300, there was some doubt as to their validity for the -5 configuration. In particular, it was not known how much effect an error in the downwash prediction might have on the study results. Therefore, a flow field survey in the neighborhood of the horizontal tail was undertaken with the Woodward program flow visualization option in order to establish confidence in the estimated downwash.

The experimental data indicated that $\epsilon_o = 1.0^o$ and $d\epsilon/d\alpha = 0.25$ were reasonable values, and they were used in all the trim drag analyses. It was assumed that because the downwash was small at cruise, the configuration perturbations would not change it sufficiently to warrant an extensive downwash investigation on each configuration. The flow visualization served to confirm these assumptions.

The downwash survey was made in six horizontal planes at different vertical heights as shown in figure 33. The vertical locations of the tail covered the space roughly between the wing plane (low) and the tail plane (high). A set of 12 downwash values were determined in each horizontal plane at the grid points shown in the inset in figure 33. This was necessary because individual Woodward off-body points were subject to scatter due to the influence of pressure discontinuities on nearby body and and wing panels. The 12 values were averaged to give an average downwash at the horizontal tail, $\bar{\epsilon}$.

The survey was run at $\alpha = 0^o$ and at $\alpha = 1.0^o$ in order to determine $d\bar{\epsilon}/d\alpha$.

The survey was run on the baseline -5 configuration. It was also run on the configuration with the 53 percent C_R constrained wing in order to check how much the downwash changed for one of the larger changes in wing camber distribution.

The results of the downwash survey are shown in figure 34. The downwash in the plane of the wing came quite close to the experimental values for both configurations. In particular, $\bar{\epsilon}_o$ showed excellent agreement. As the downwash was sampled higher above the wing plane, $\bar{\epsilon}_o$ and $d\bar{\epsilon}/d\alpha$ tended toward slightly higher values of 1.4^o and 0.40 respectively.

The plane-of-the-wing downwash values were determined to be acceptable particularly in light of their agreement with the experimental values. It is interesting to note that the tail-on methods of Carlson and Middleton (refs. 6 and 7) use planar downwash.

However, it was considered possible that the Woodward values in the plane of the tail more accurately represented the downwash in the three-dimensional flow field. So, the higher values of $\bar{\epsilon}_o = 1.4^o$ and $d\bar{\epsilon}/d\alpha = 0.4$ were used to check the sensitivity of the baseline configuration trim analyis to uncertainity in knowledge of the downwash. The results of this sensitivity study are shown in figure 35. The change in L/D at the nominal center of gravity location is only about 0.03 for the worst case. On this basis, it was decided that the study was accurate in terms of the effect of downwash on the study results.

REFERENCES

1. Woodward, F.A.; Tinoco, E.N.; and Larsen, J.W.: Analysis and Design of Supersonic Wing-Body Combinations, Including Flow Properties in the Near Field. NASA CR-73106, 1967.

2. Gentry, Arvel, E.; Smyth, Douglas N.; and Oliver, Wayne R.: Hypersonic Arbitrary Body Aerodynamic Computer Program. Douglas Aircraft Company Report 61558, April 1968.

3. Gentry, Arvel E.; Smyth, Douglas N.; and Oliver, Wayne R.: User's Manual for the Mark IV Version of the Supersonic-Hypersonic Arbitrary Body Program. Prepared for AFFDL under contract F33615-72-C-1675, November 1973.

4. Clutter, Darwin W.: Charts for Determining Skin Friction Coefficients on Smooth and on Rough Flat Plates at Mach Numbers Up to 5.0 With and Without Heat Transfer. Douglas Aircraft Company Report ES 29074, April 1959.

5. Baals, Donald D; Robins, A. Warner; and Harris, Roy V.; Aerodynamic Design Integration of Supersonic Aircraft. AIAA Paper No. 68-1018, October 1968.

6. Carlson, Harry W.; and Middleton, Wilbur D.: A Numerical Method for the Design of Camber Surfaces of Supersonic Wings with Arbitrary Planforms. NASA TN D-2341, 1964.

7. Middleton, Wilber D., and Carlson, Harry W.: Numerical Method of Estimating and Optimizing Supersonic Aerodynamic Characteristics of Arbitrary Planform Wings. J. Aircraft, Volume 2, No. 4, July-August 1965, pp. 261-265.

D-3230-2.2-5

S_W = 928 sq m (10,000 sq ft)

S_t = 72.5 sq m (781 sq ft)

AR_w = 1.84

AR_t = 2.00

273 PASSENGERS

RANGE = 7408 km (4000 n mi)

DIMENSIONS: METERS
(INCHES)

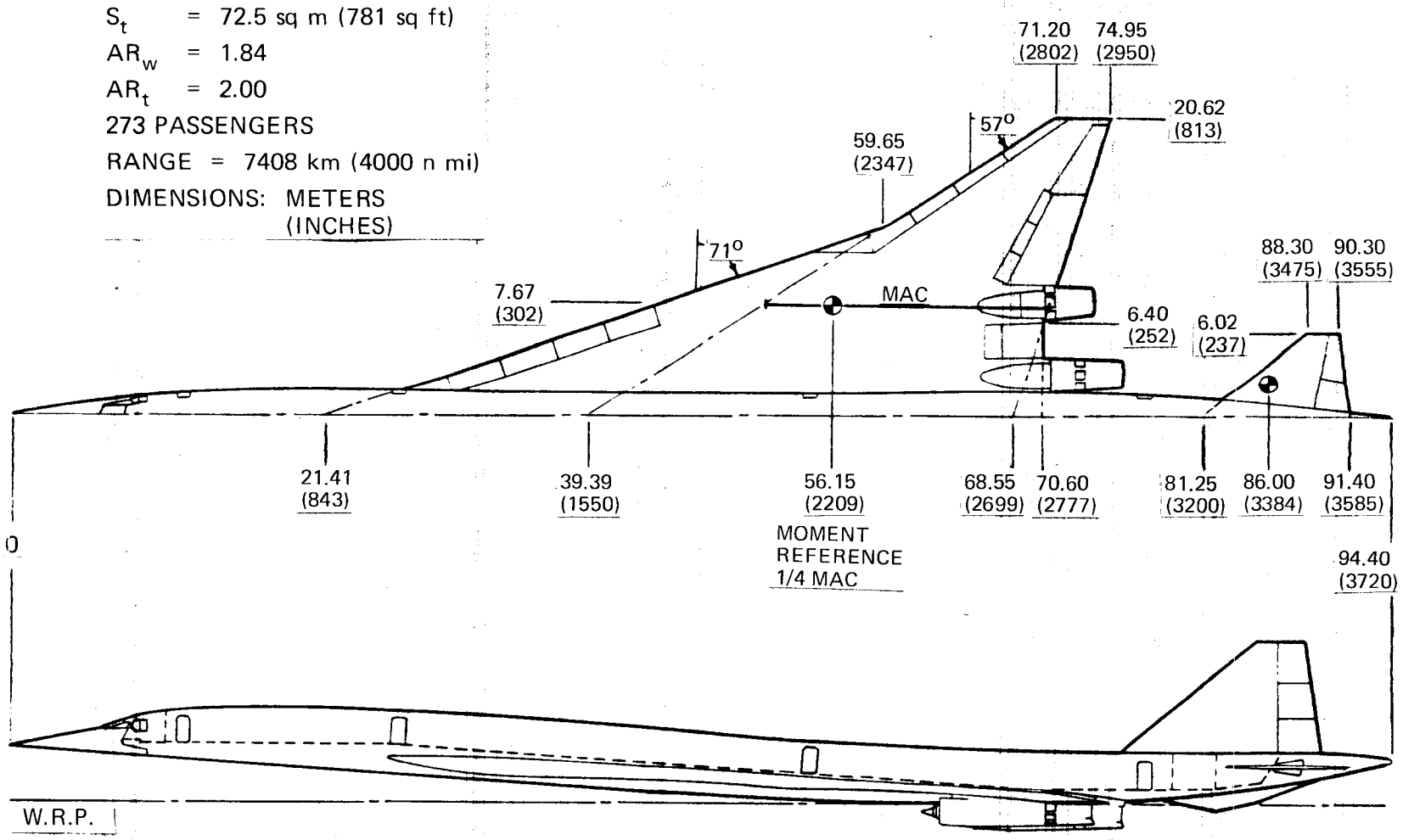

Figure 1. General Arrangement of the Douglas D-3230-2.2-5 Baseline Configuration

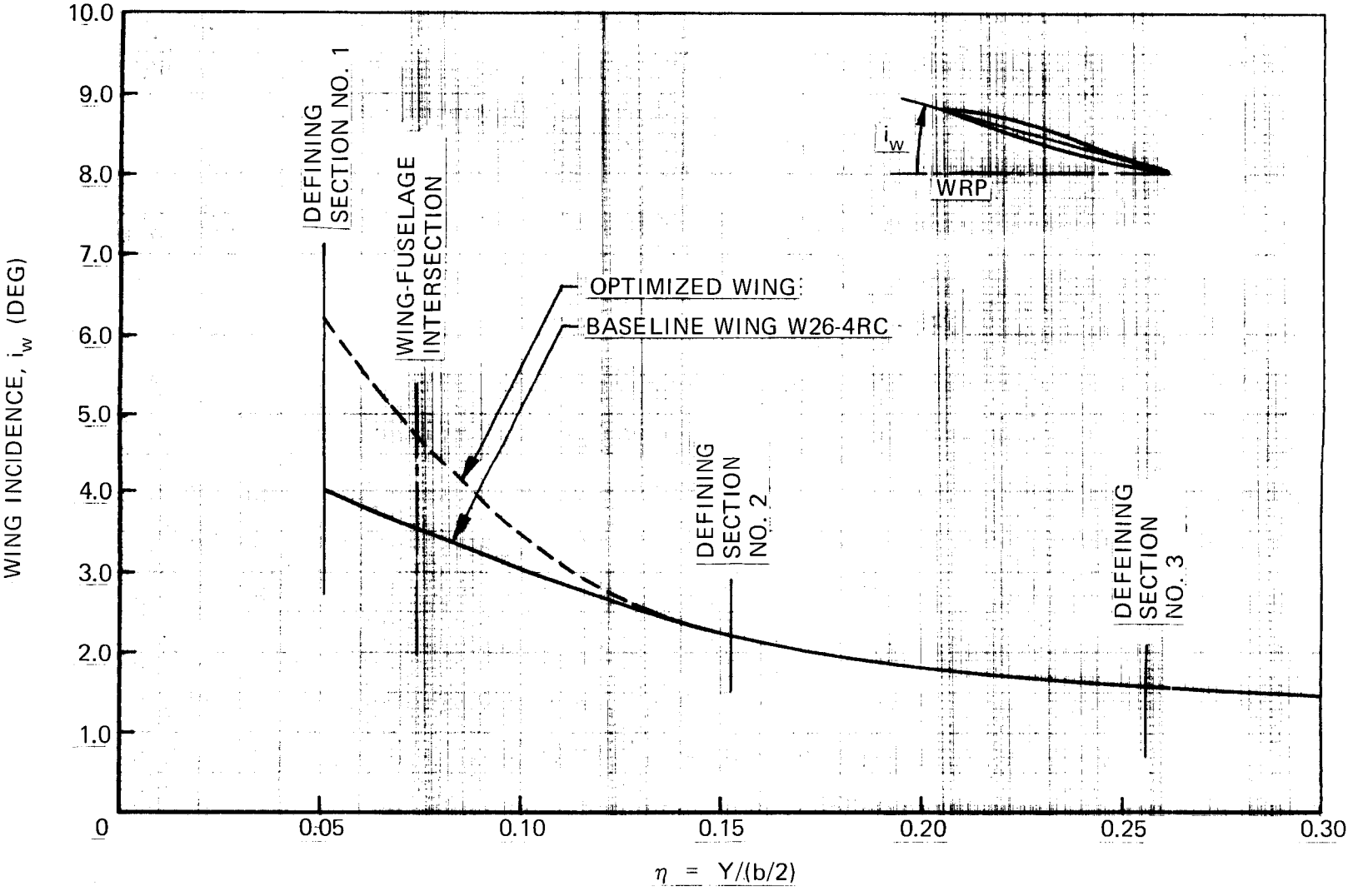

Figure 2. Inboard Wing Incidence for the Baseline and Optimum Wings

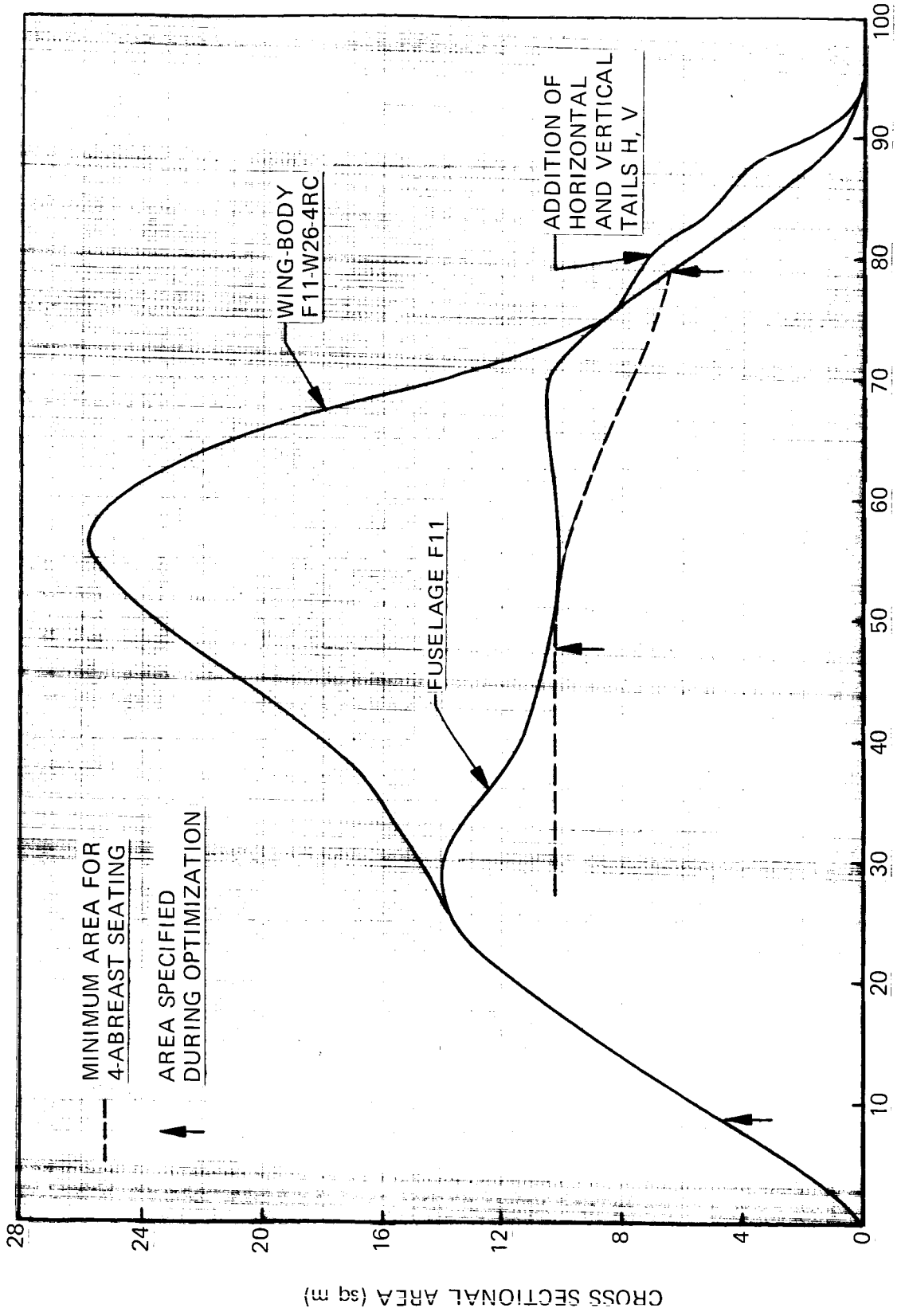

Figure 3. Normal (M = 1.0) Cross Sectional Area Distribution for the D-3230-2.2-5

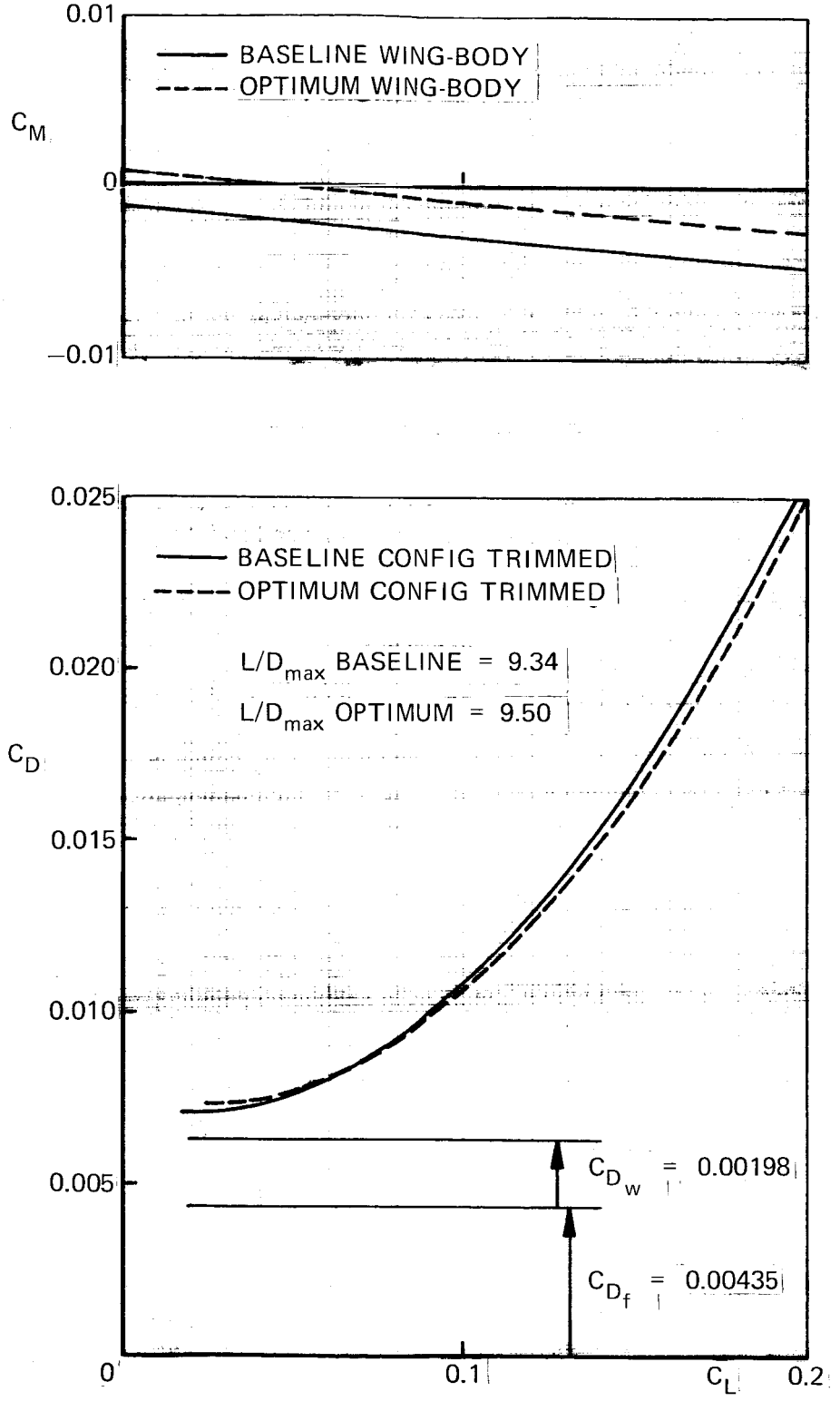

Figure 4. Pitching Moment Coefficient and Drag Coefficient vs Lift Coefficient for the Optimum and Baseline Configurations

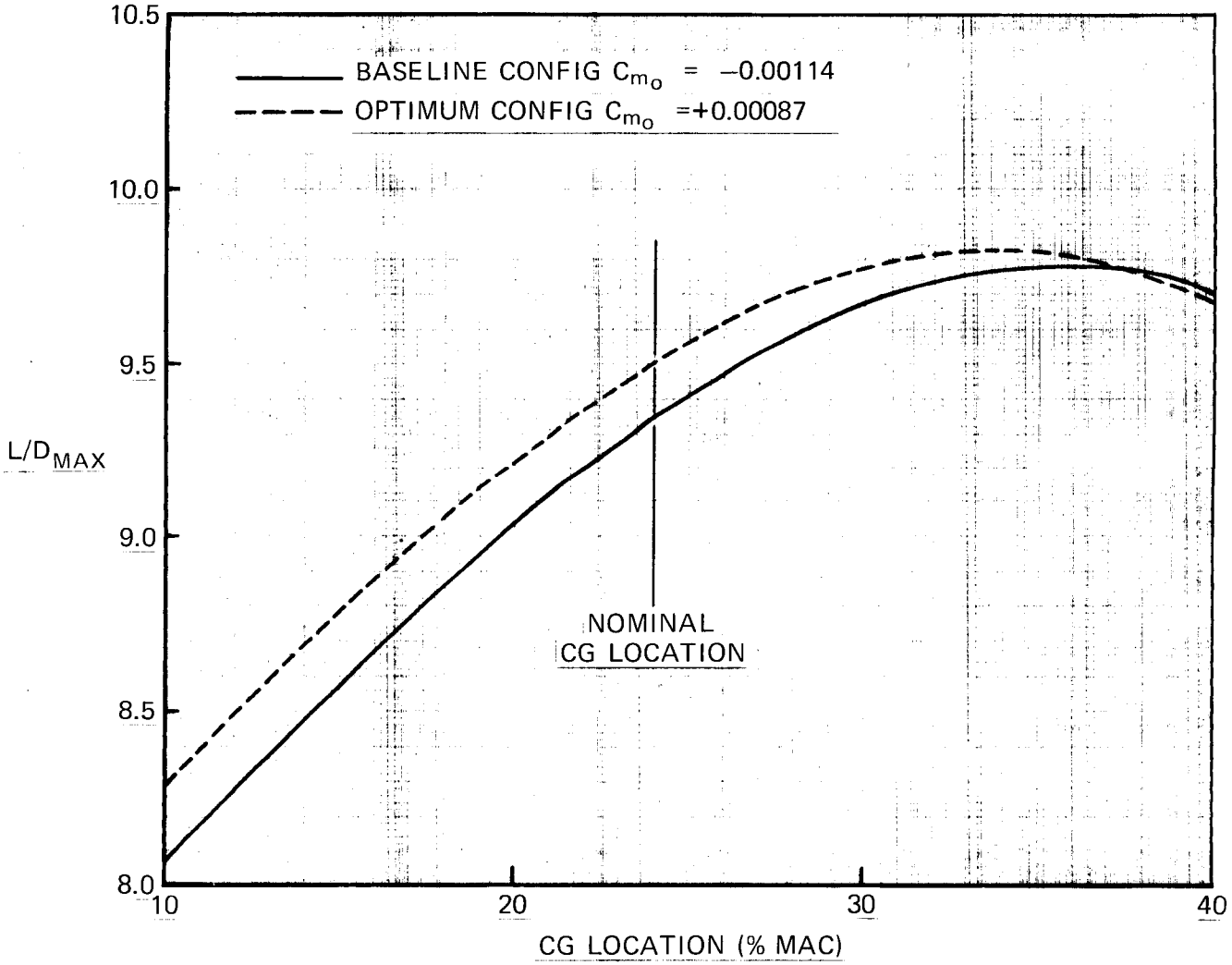

Figure 5. L/D_{max} vs Center-of-Gravity Location for the Optimum and Baseline Configurations

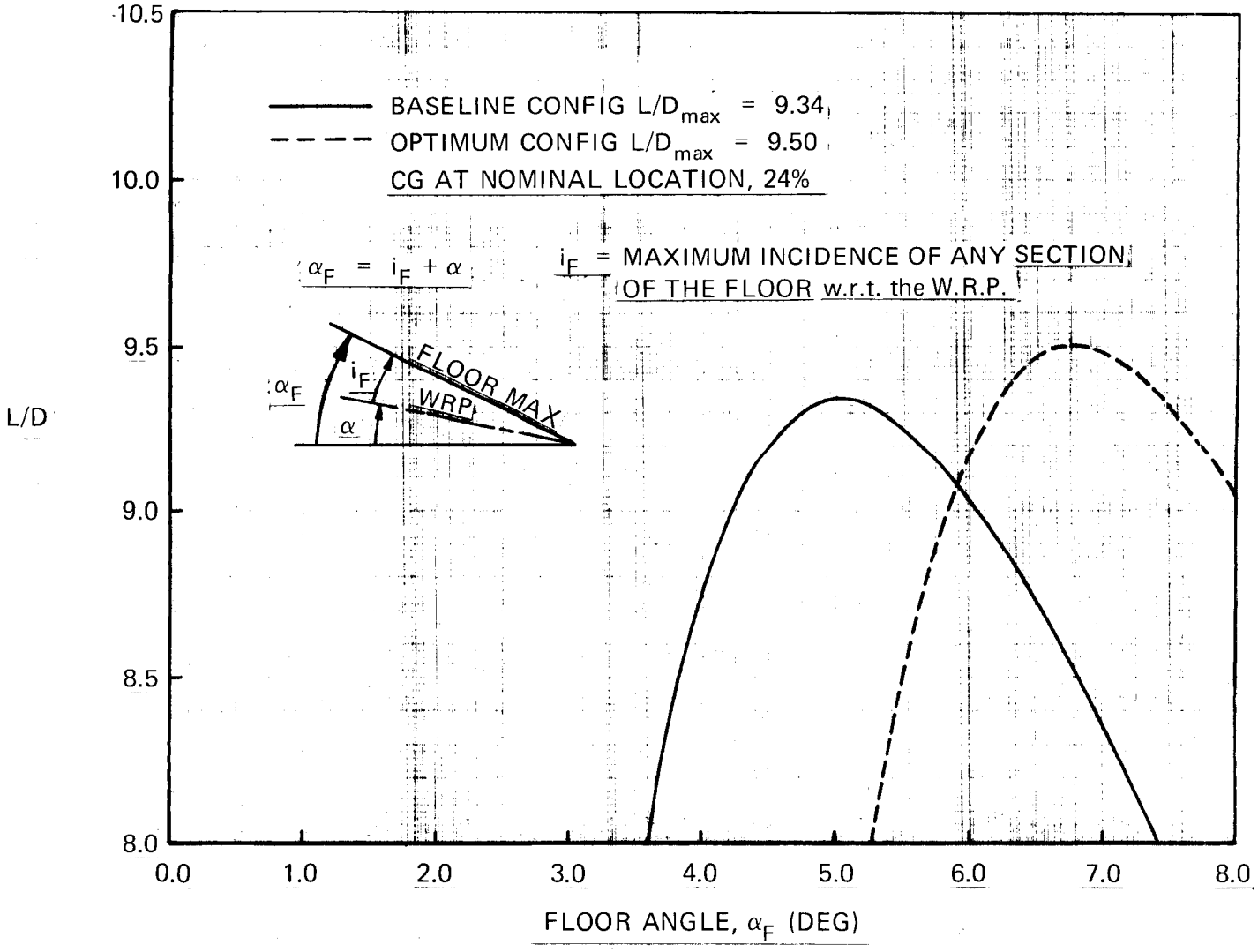

Figure 6. L/D vs Floor Angle for the Optimum and Baseline Configurations with the cg at 24% MAC (Nominal)

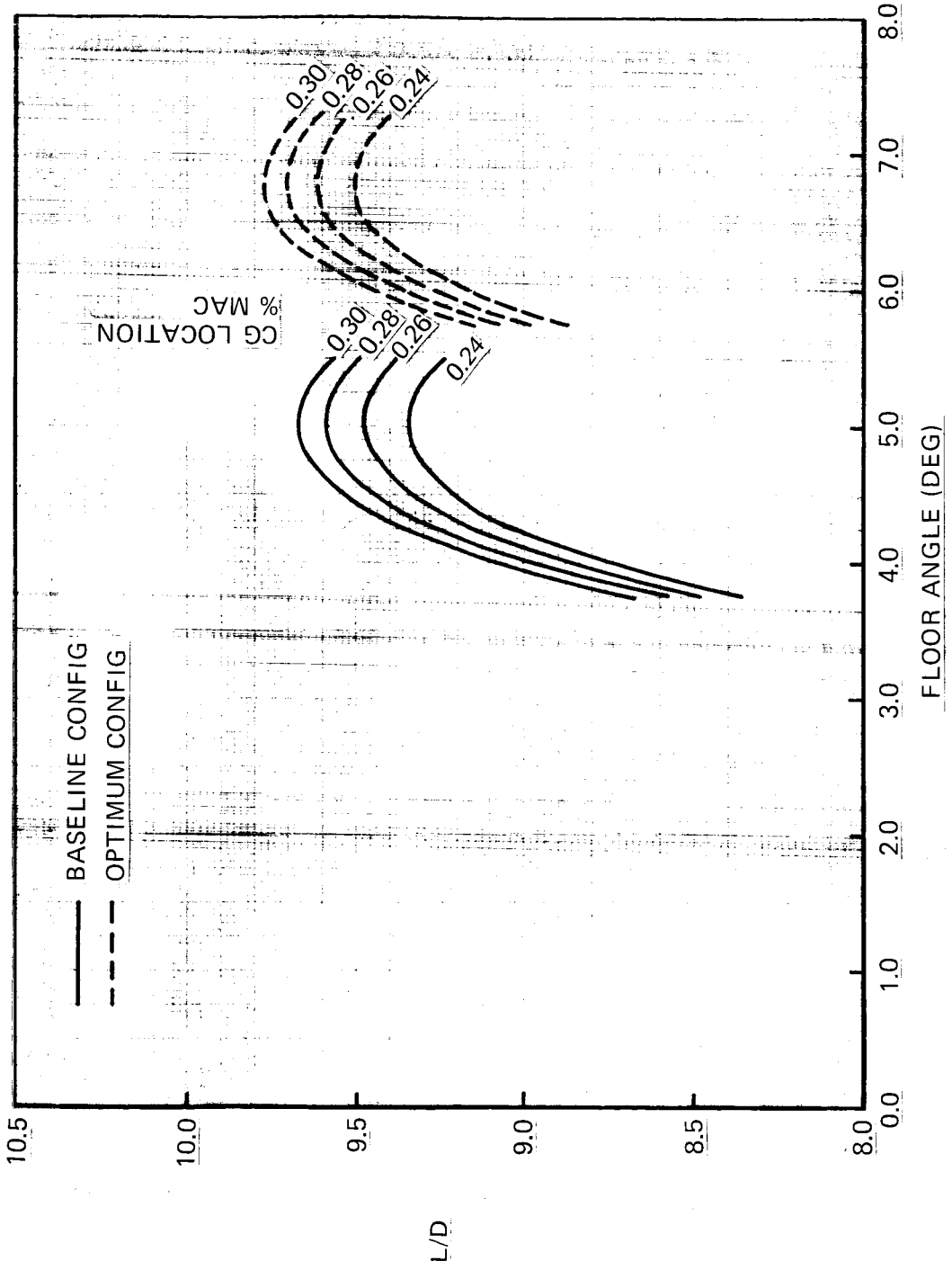

Figure 7. Effect of Aft cg Movement on L/D vs Floor Angle for the Optimum and Baseline Configurations

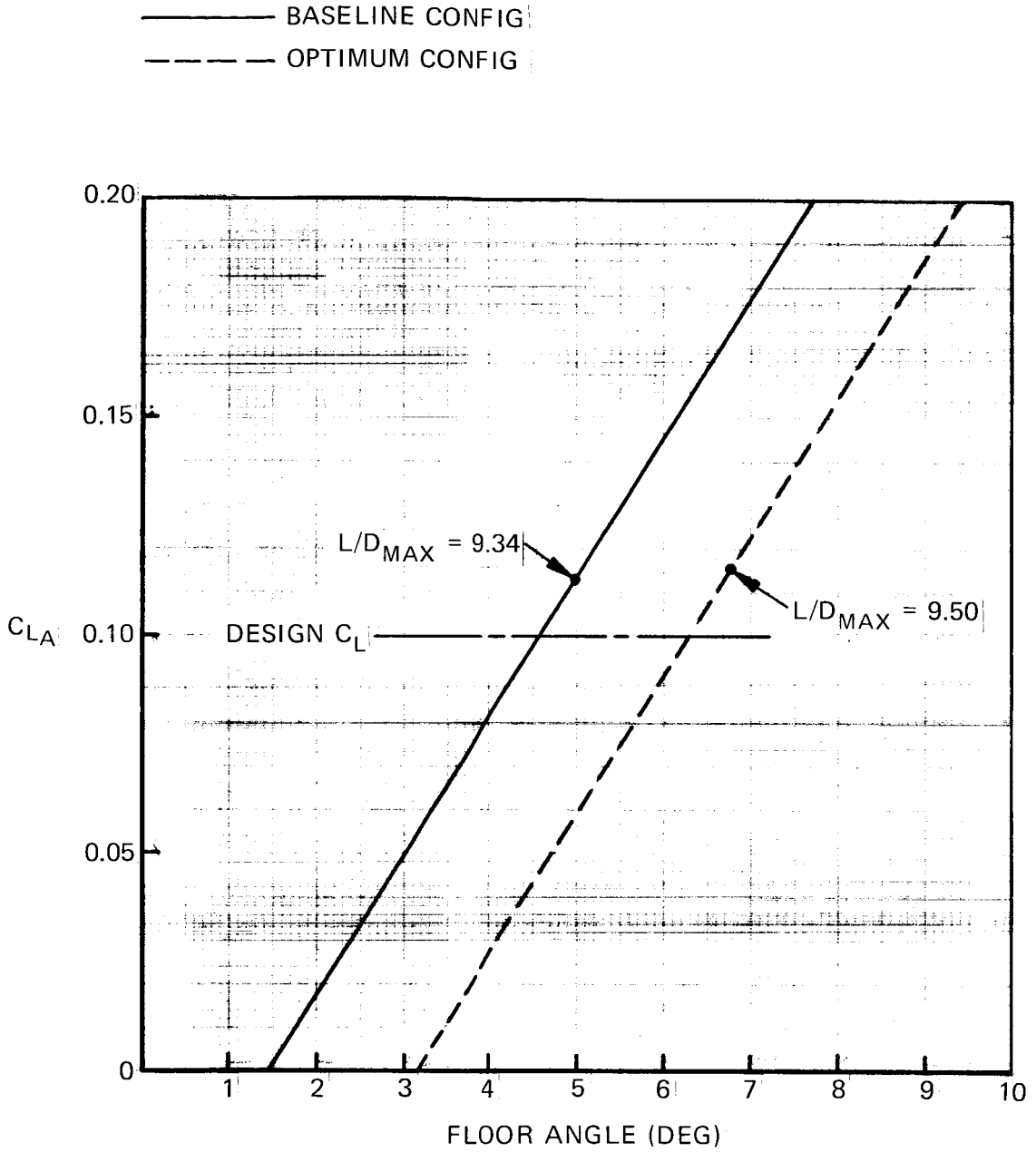

Figure 8. Lift Coefficient vs Floor Angle for the Optimum and Baseline Configurations

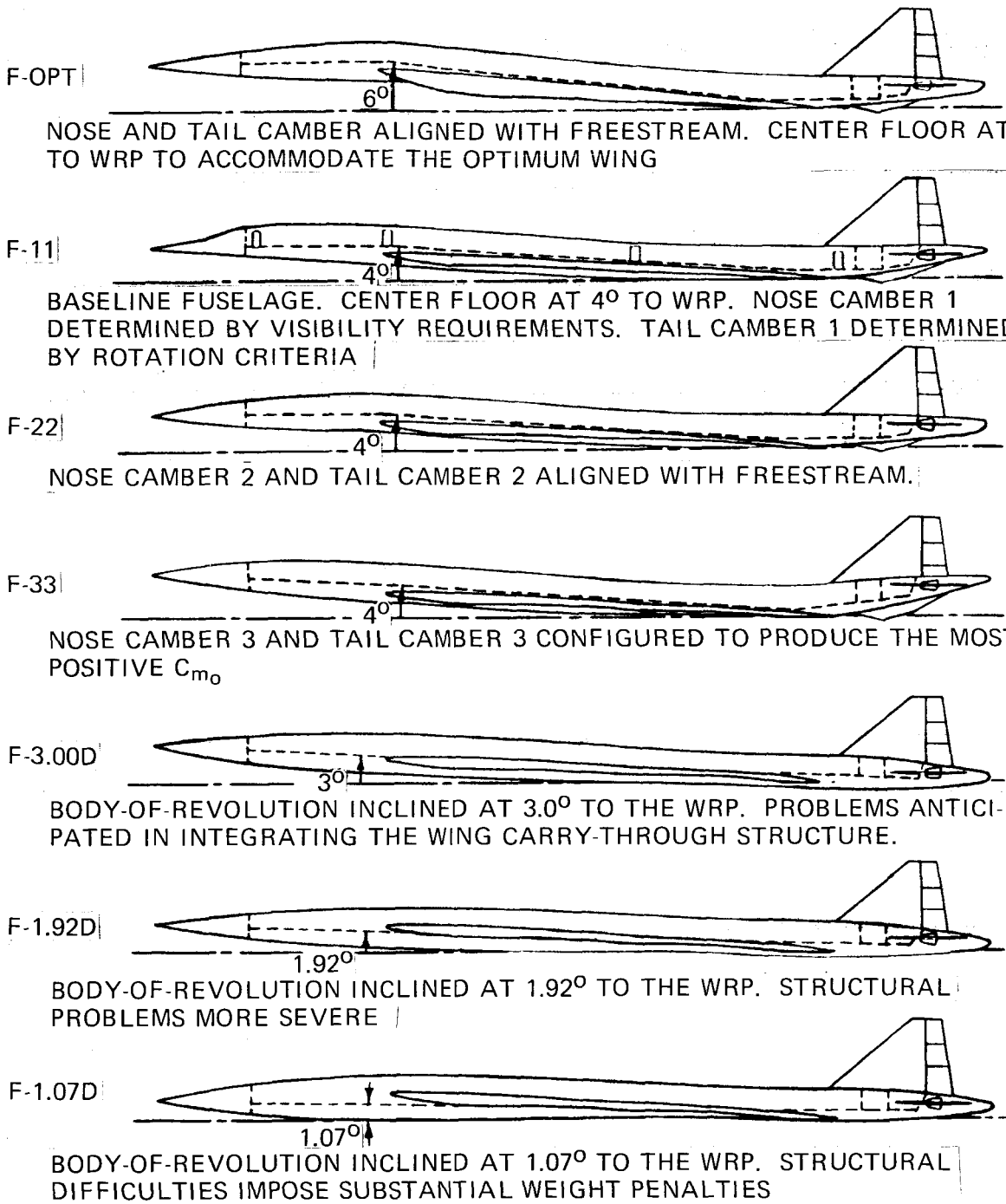

Figure 9. Schematic Representation of the Fuselage Camber Variations Studied

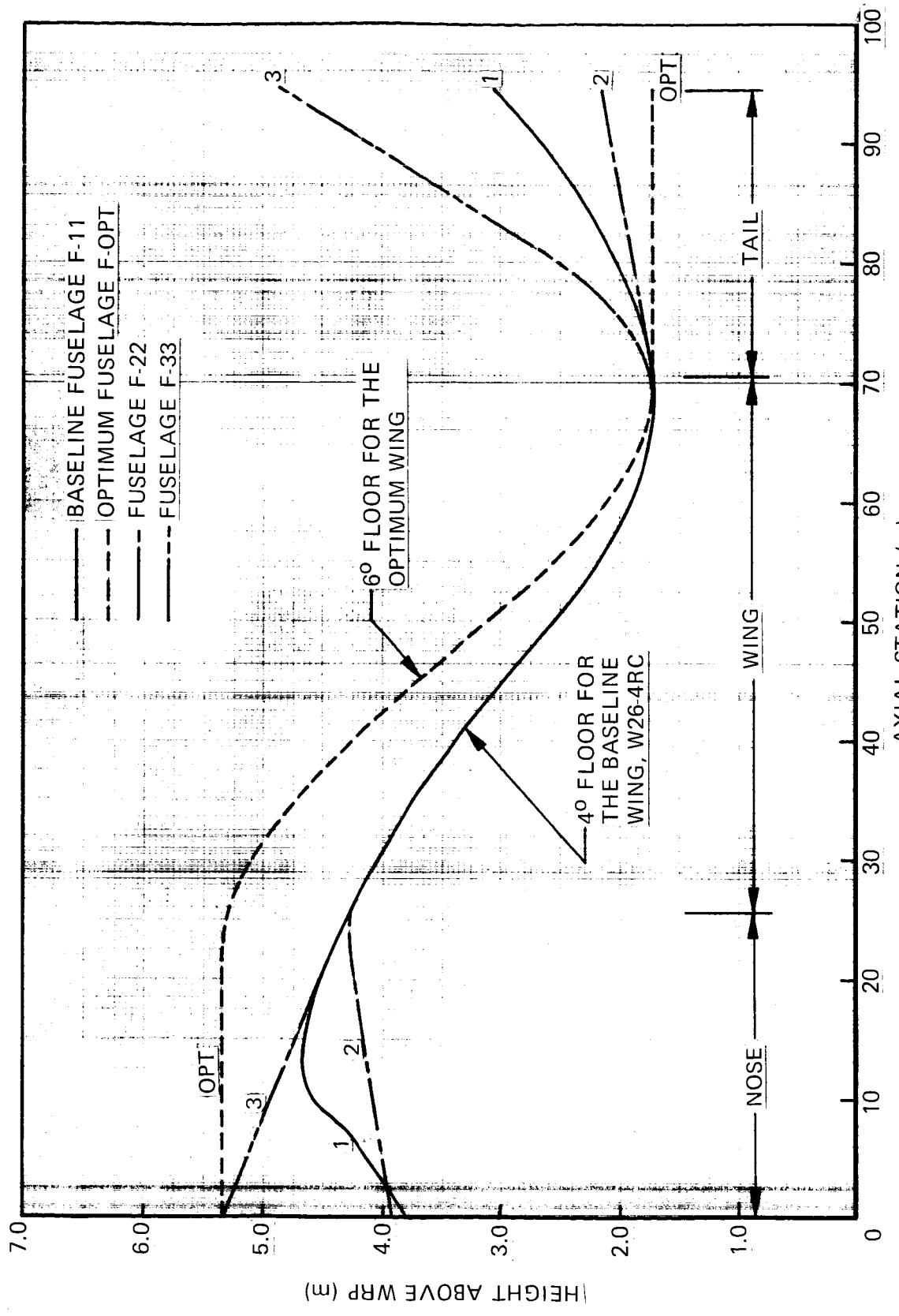

Figure 10. Fuselage Camber Line Details

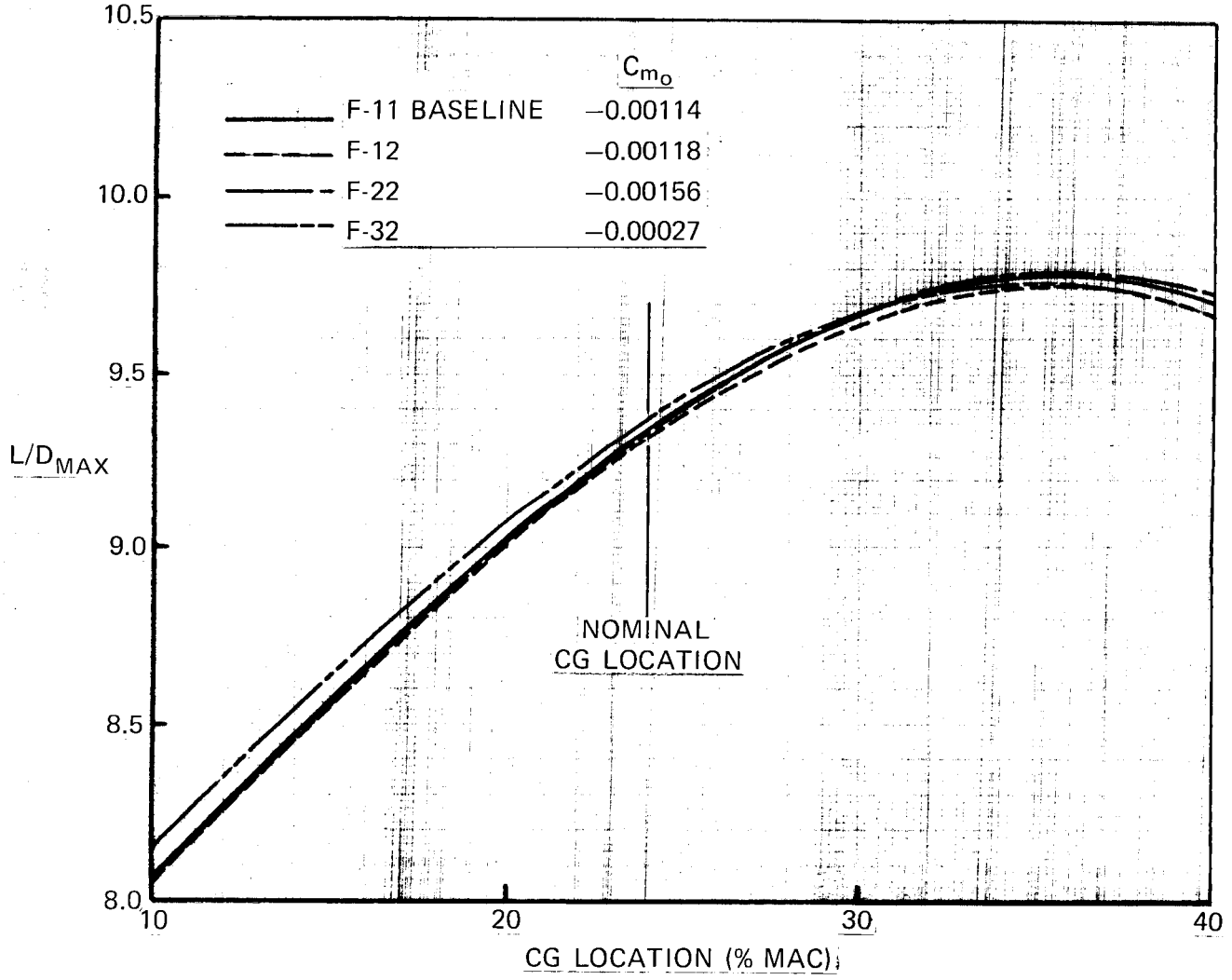

Figure 11. Effect of Nose Camber Variations on L/D_{max} vs Center-of-Gravity Location

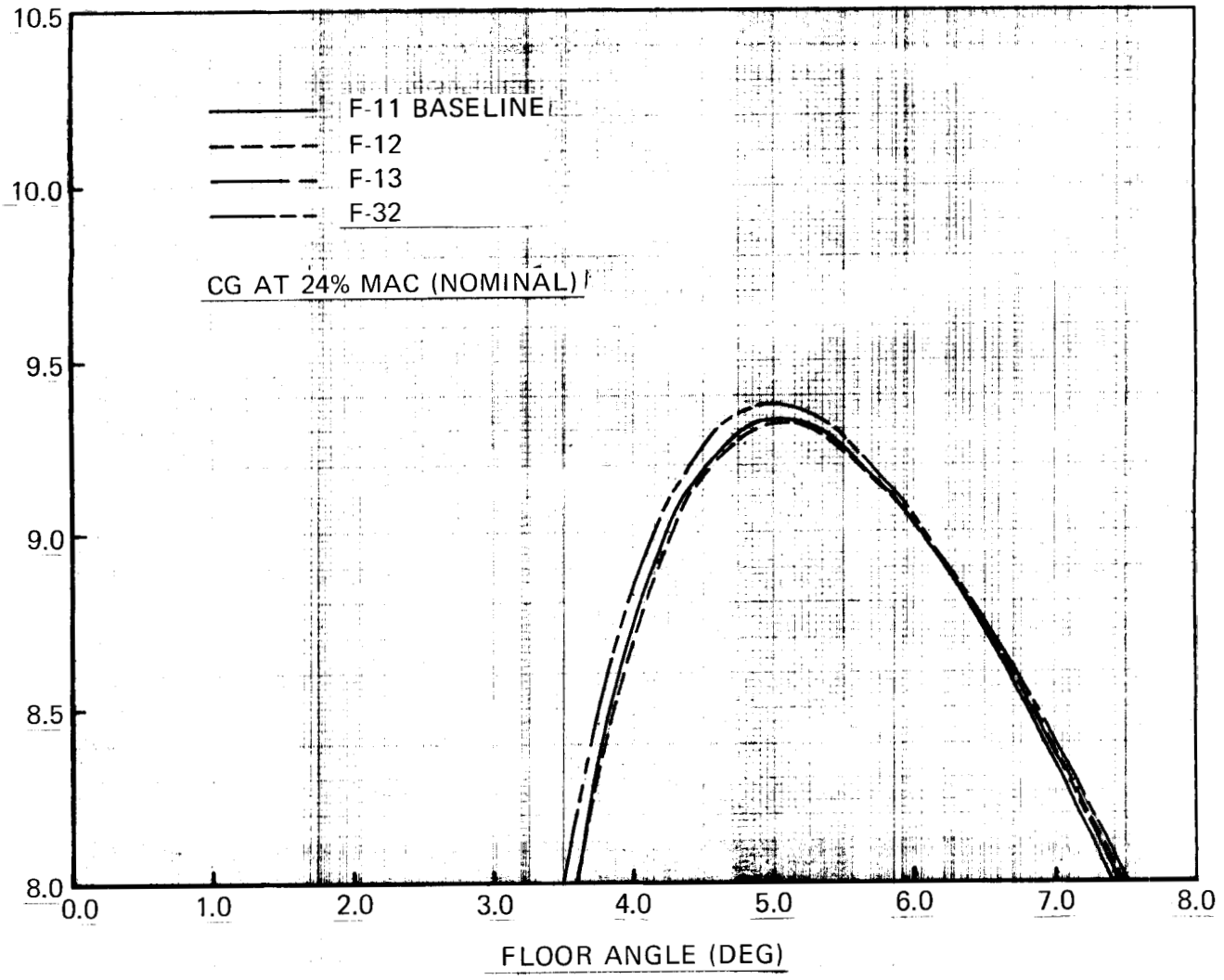

Figure 12. Effect of Nose Camber Variations on L/D vs Floor Angle for the CG at 24% MAC (Nominal)

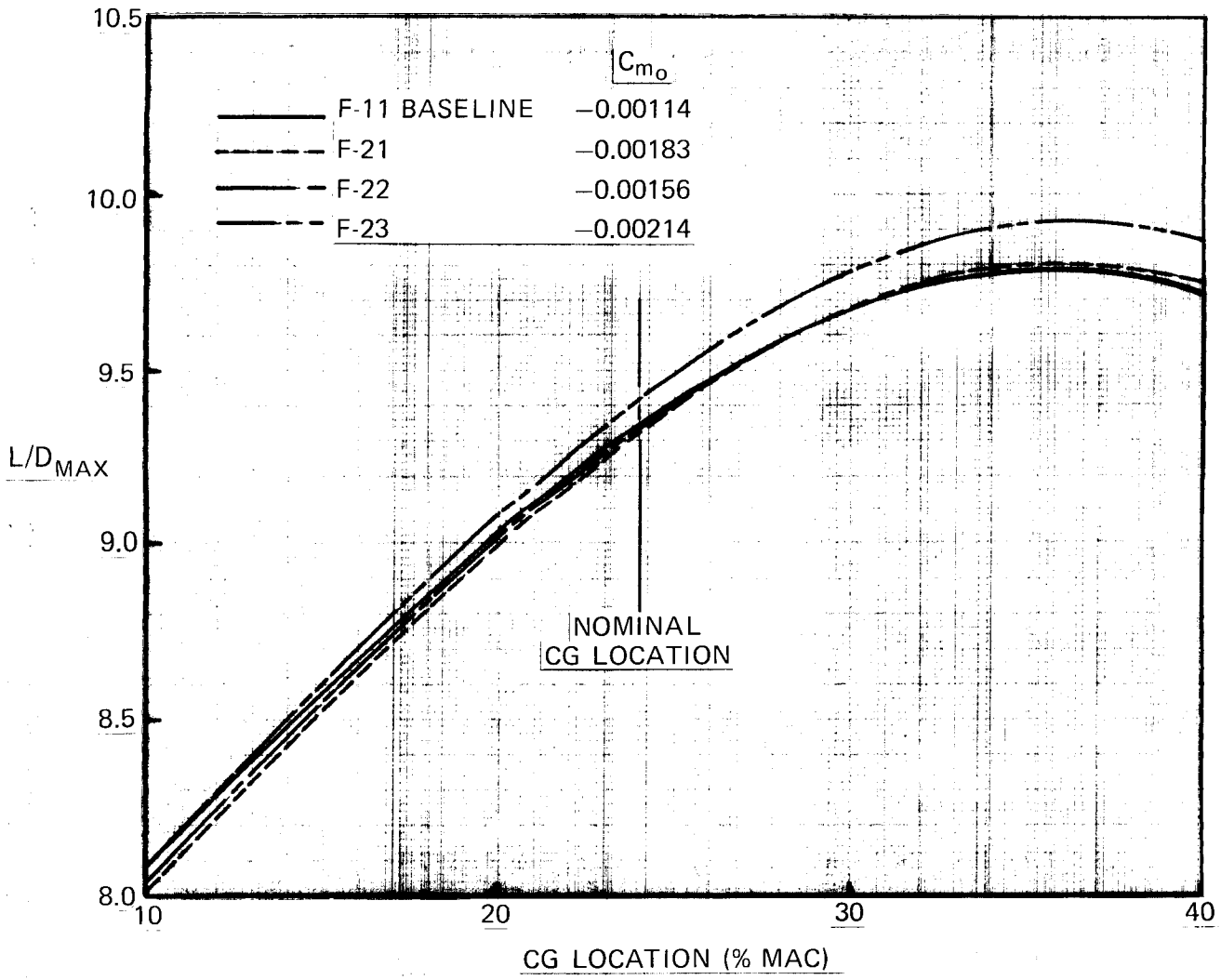

Figure 13. Effect of Tail Camber Variations on L/D_{max} vs Center-of-Gravity Location

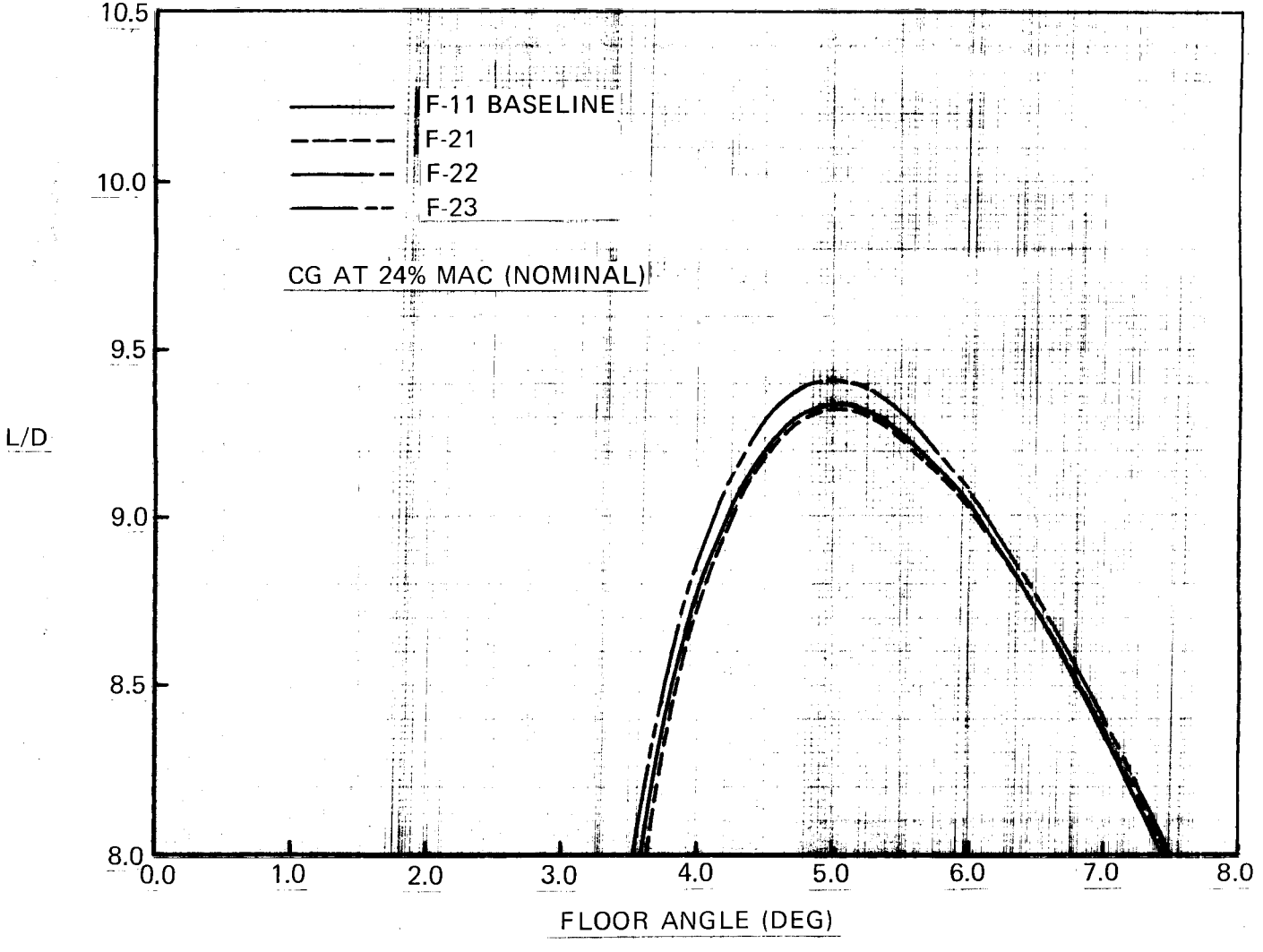

Figure 14. Effect of Tail Camber Variations on L/D vs Floor Angle for the CG at 24% MAC (Nominal)

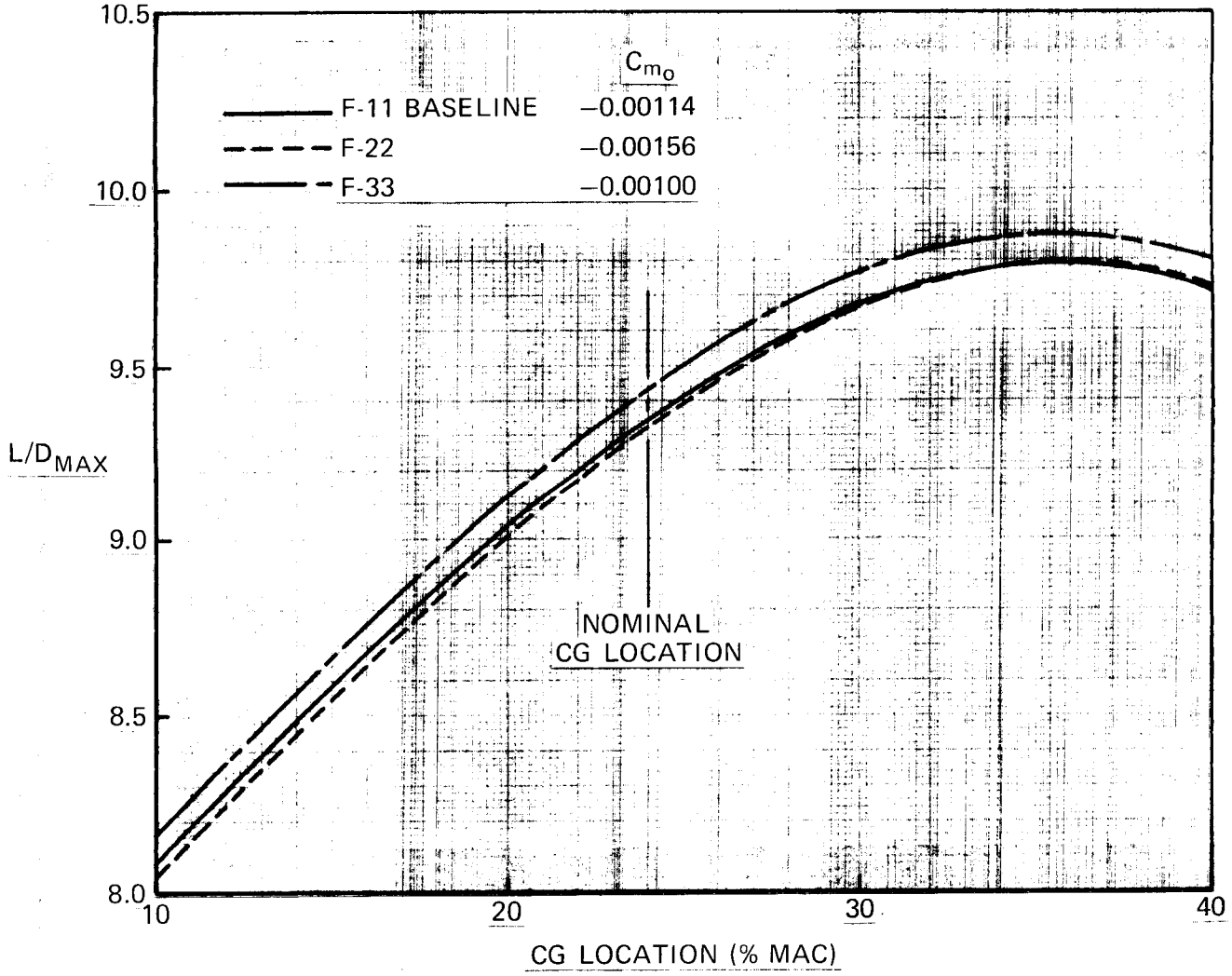

Figure 15. Combined Effect of Nose and Tail Camber Variations on L/D_{max} vs Center-of-Gravity Location

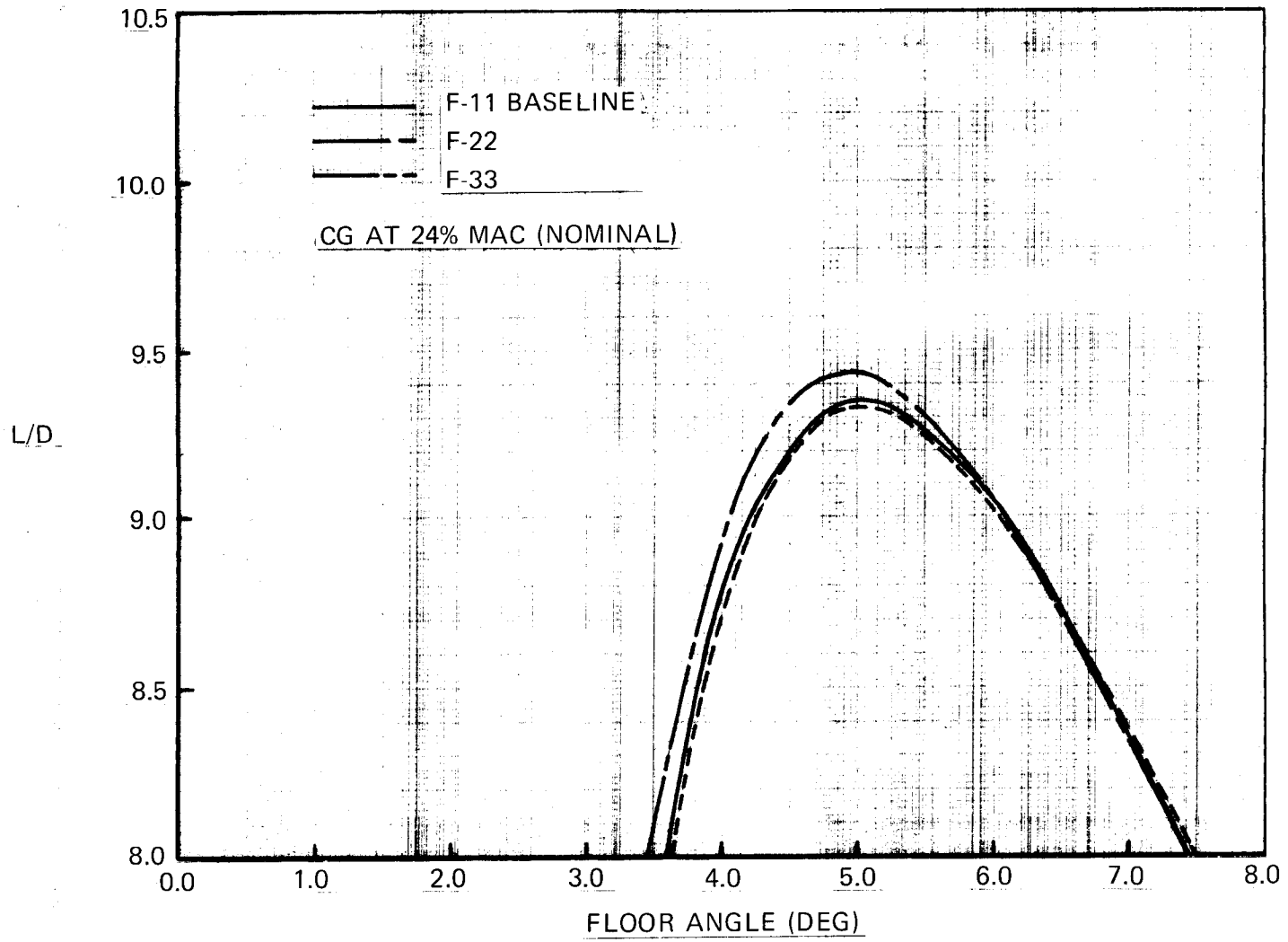

Figure 16. Combined Effect of Nose and Tail Camber Variations on L/D vs Floor Angle for the cg at 24% MAC (Nominal)

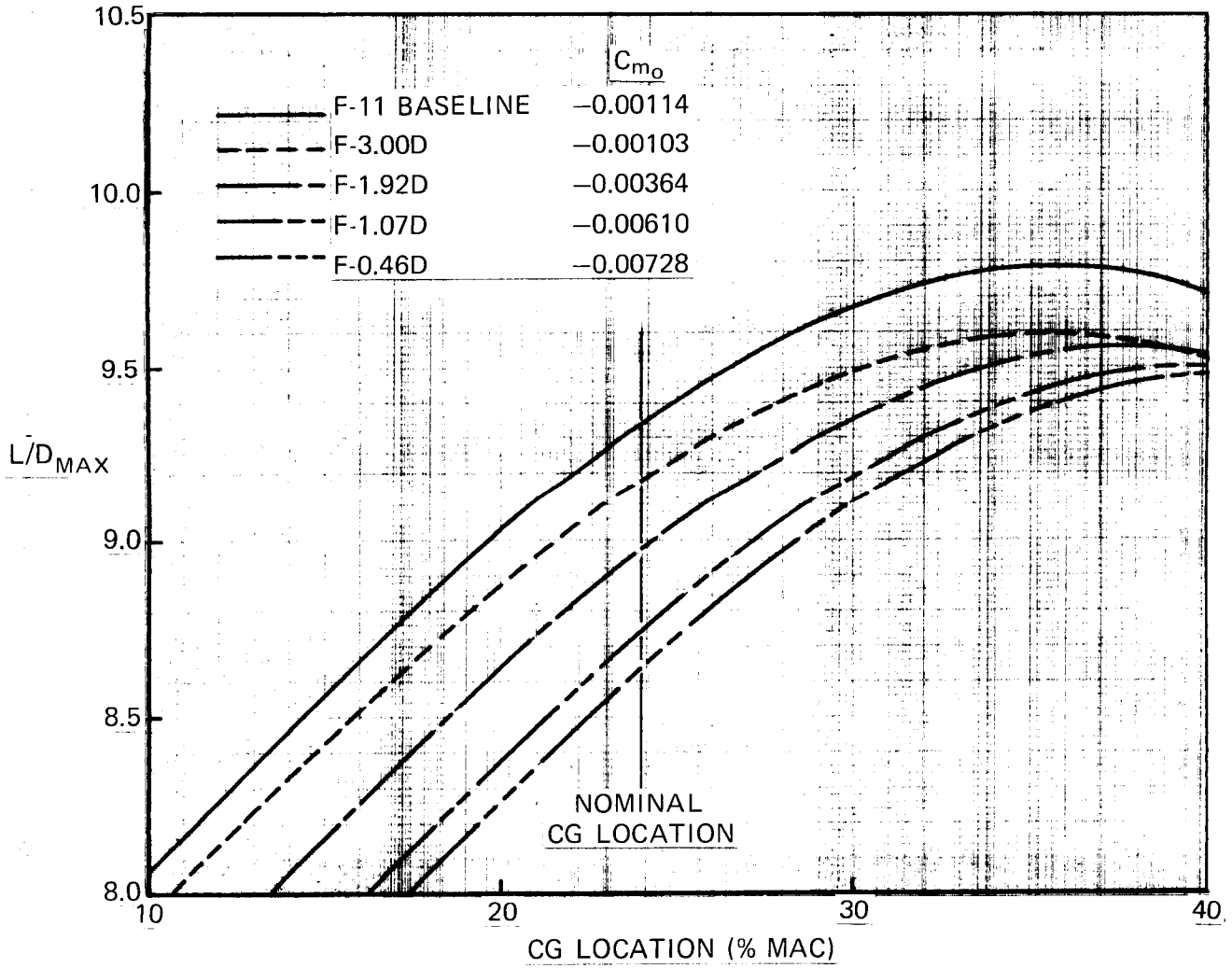

Figure 17. Effect of Reduced Fuselage Incidence on L/D_{max} vs Center-of-Gravity Location

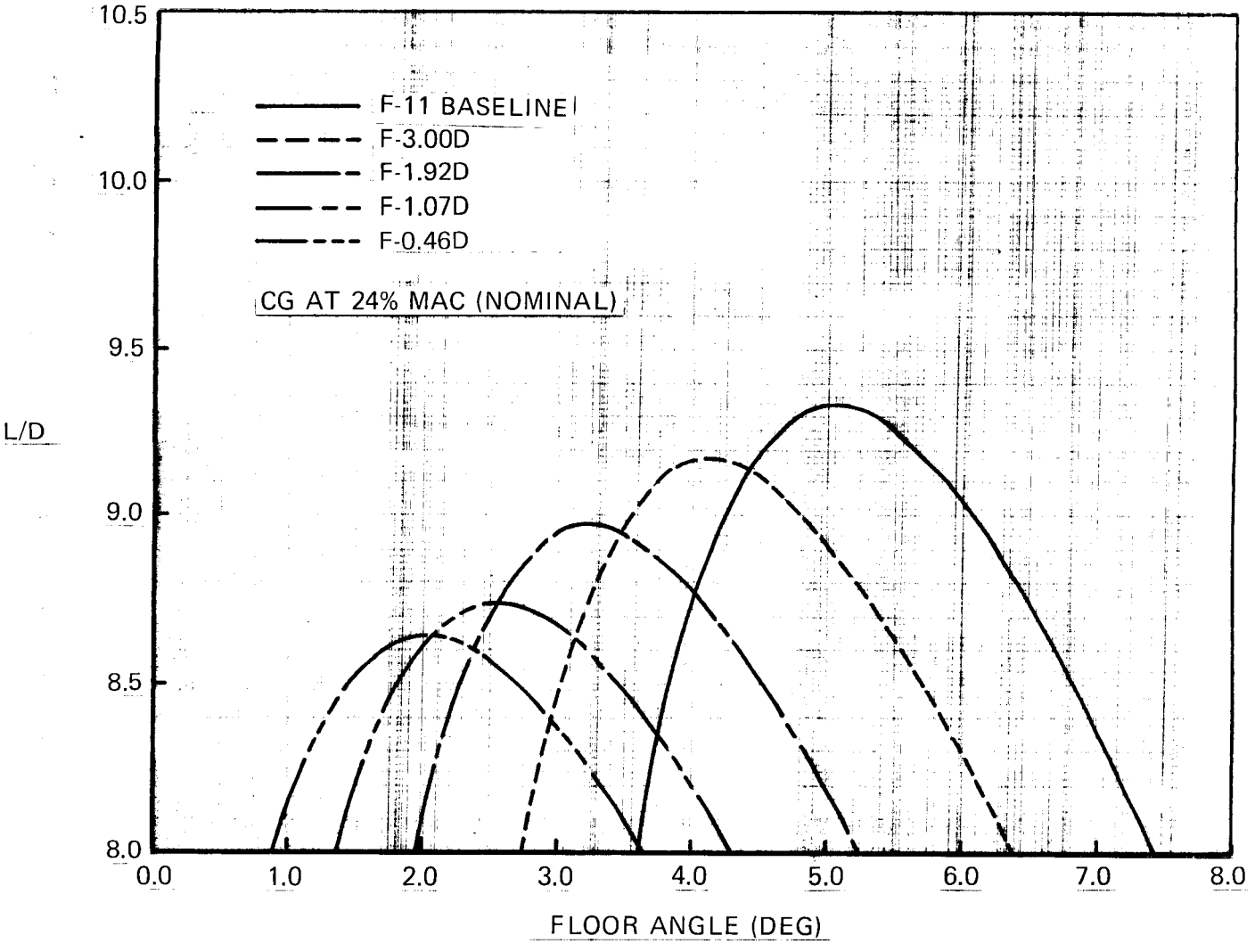

Figure 18. Effect of Reduced Fuselage Incidence on L/D vs Floor Angle With the cg at 24% MAC (Nominal)

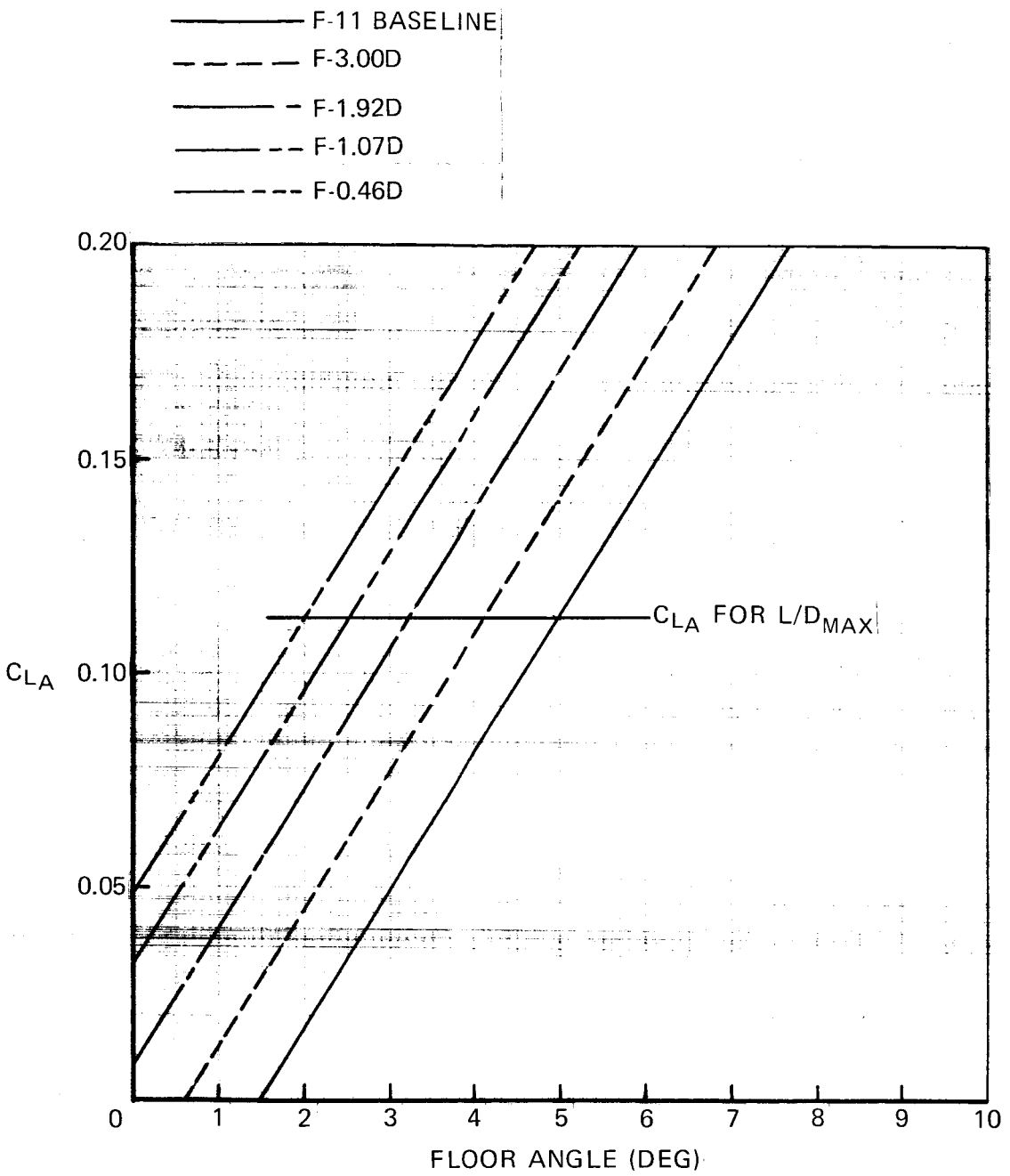

Figure 19. Lift Coefficient vs Floor Angle for Configurations With Reduced Fuselage Incidence

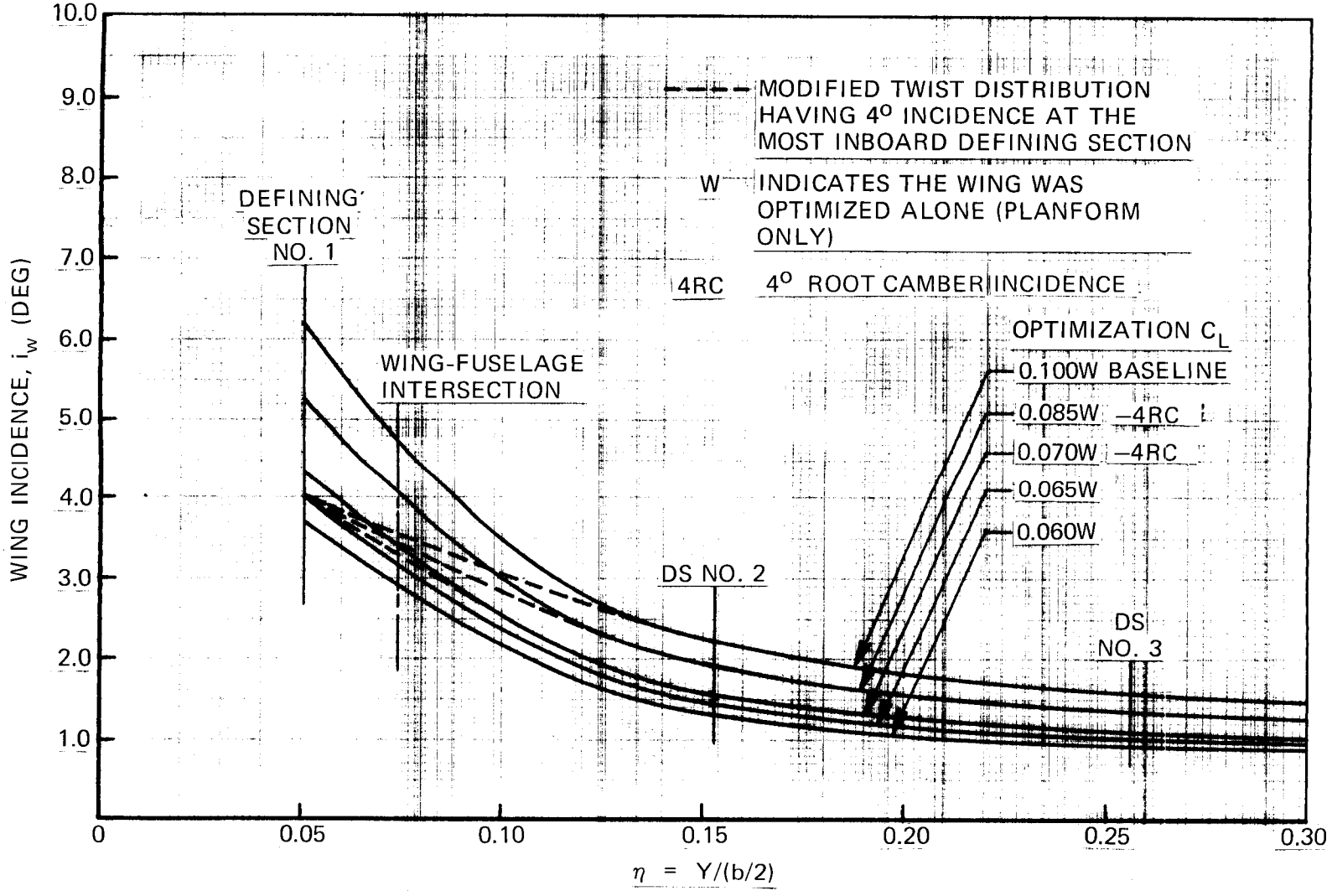

Figure 20. Inboard Wing Incidence for Wings Optimized Alone at C_L's Less Than the Design C_L

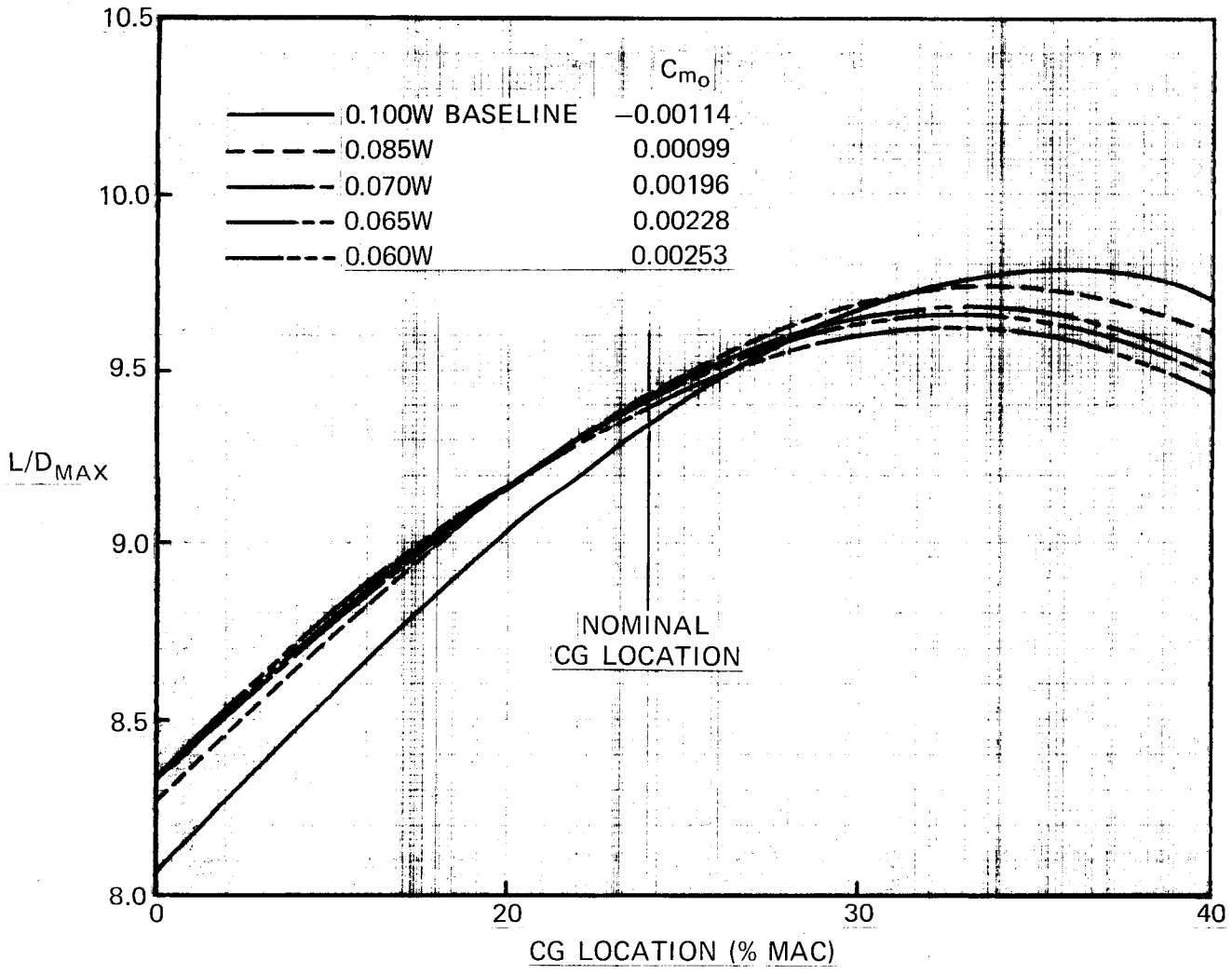

Figure 21. Effect of Low C_L Optimized Wings on L/D_{max} vs Center-of-Gravity Location

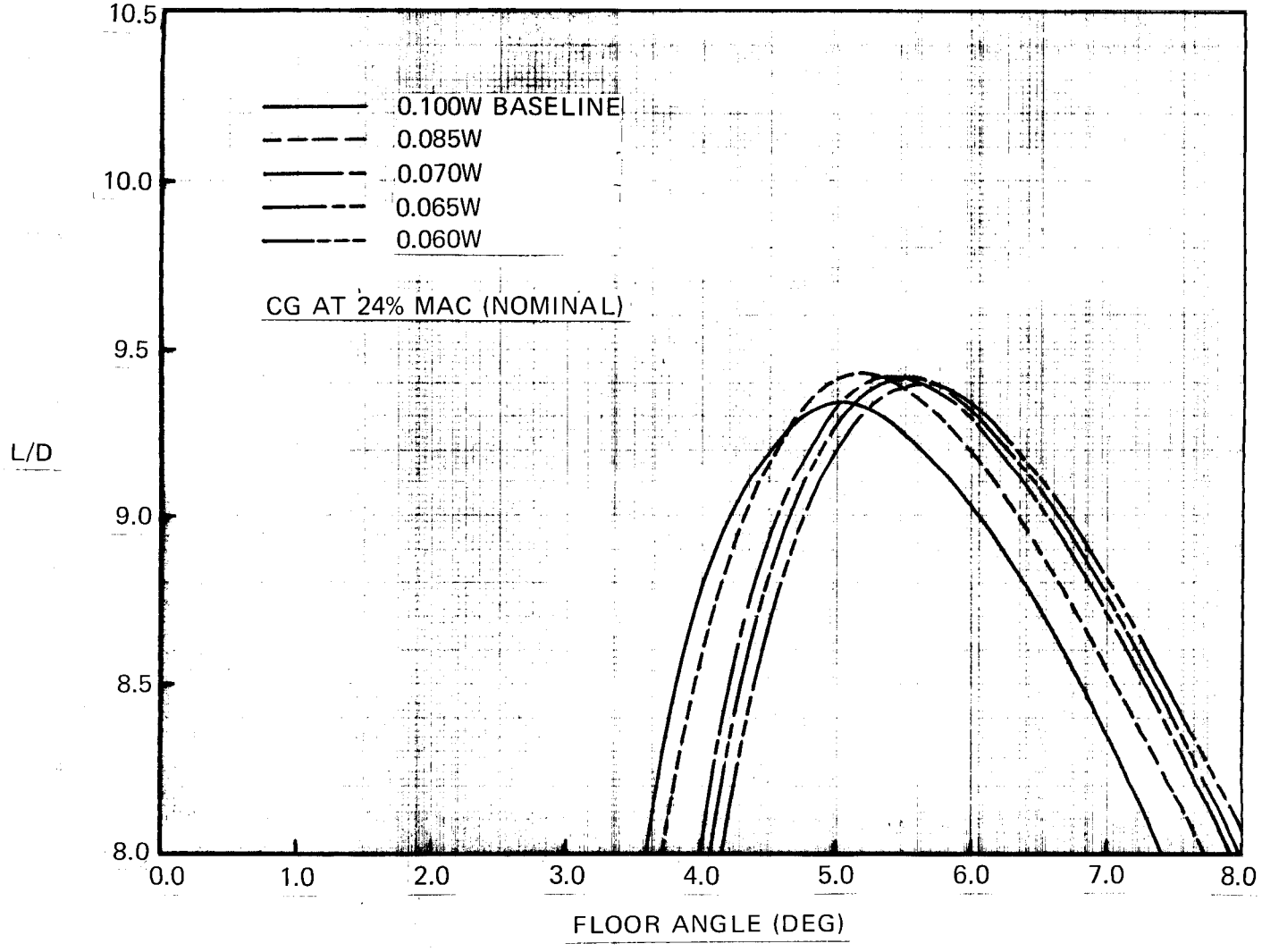

Figure 22. Effect of Low C_L Optimized Wings on L/D vs Floor Angle for the cg at 24% MAC (Nominal)

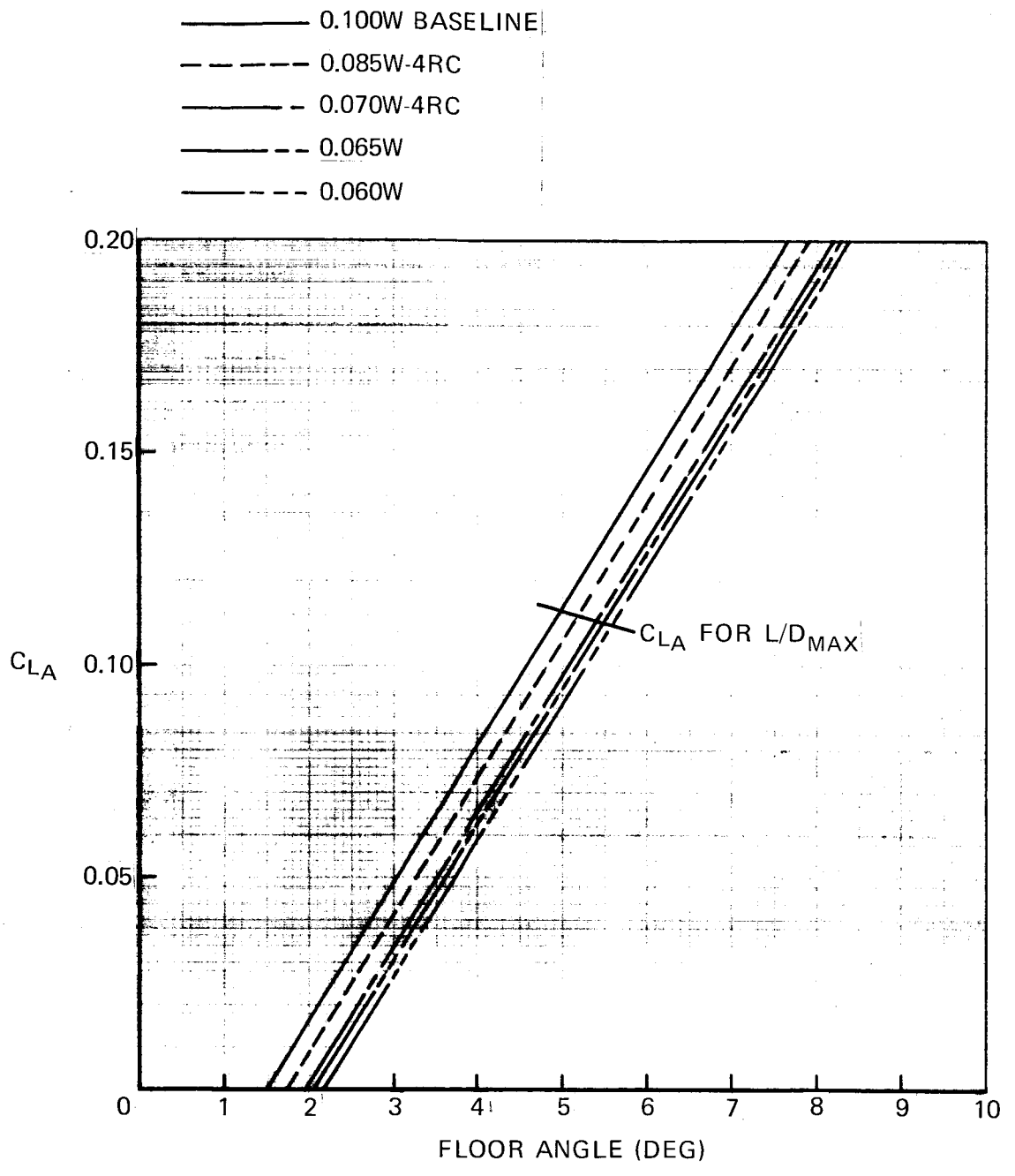

Figure 23. Lift Coefficient vs Floor Angle for Wings Optimized at C_L's Less Than the Design C_L

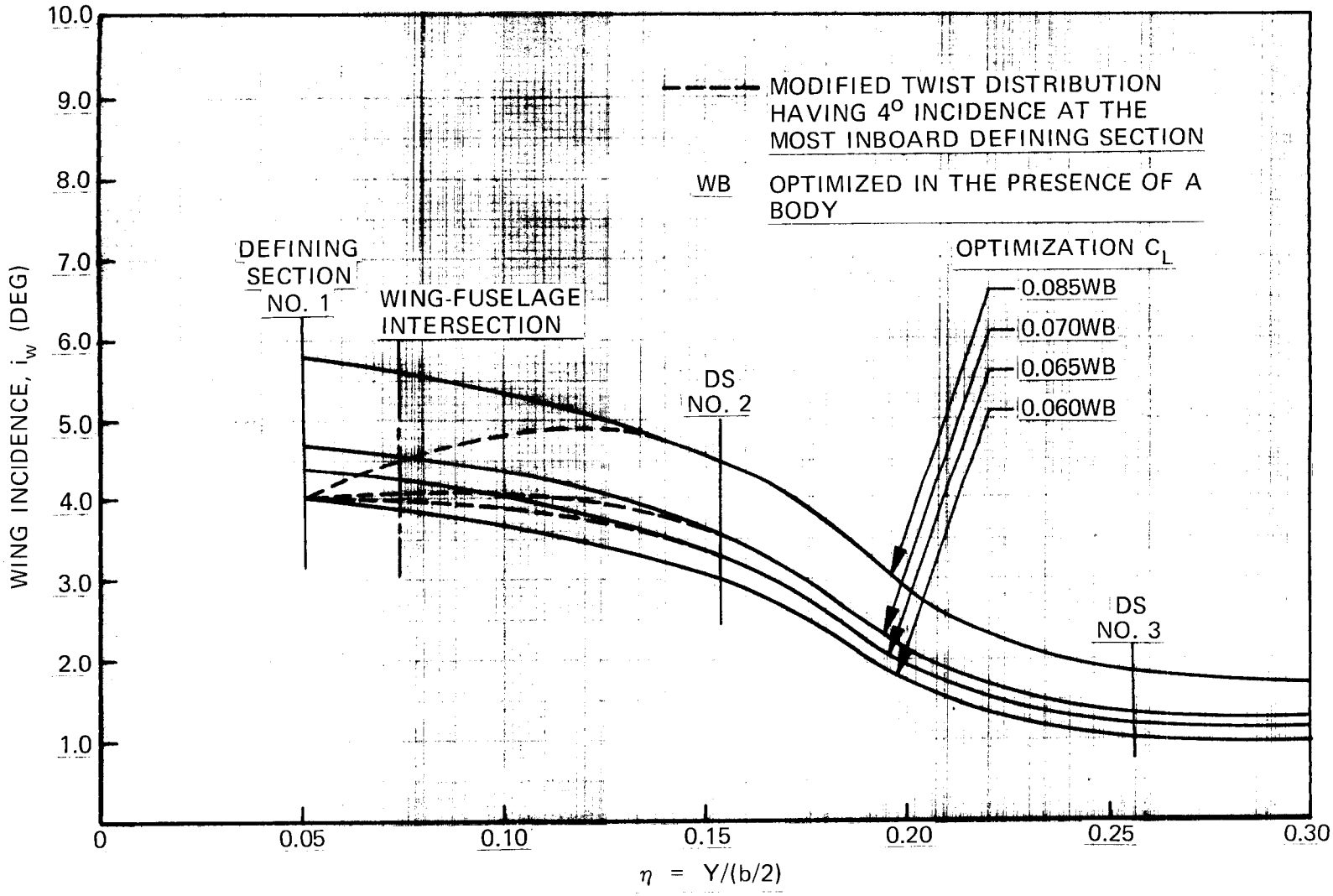

Figure 24. Inboard Wing Incidence for Wings Optimized in the Presence of a Fuselage at C_L's Less Than the Design C_L

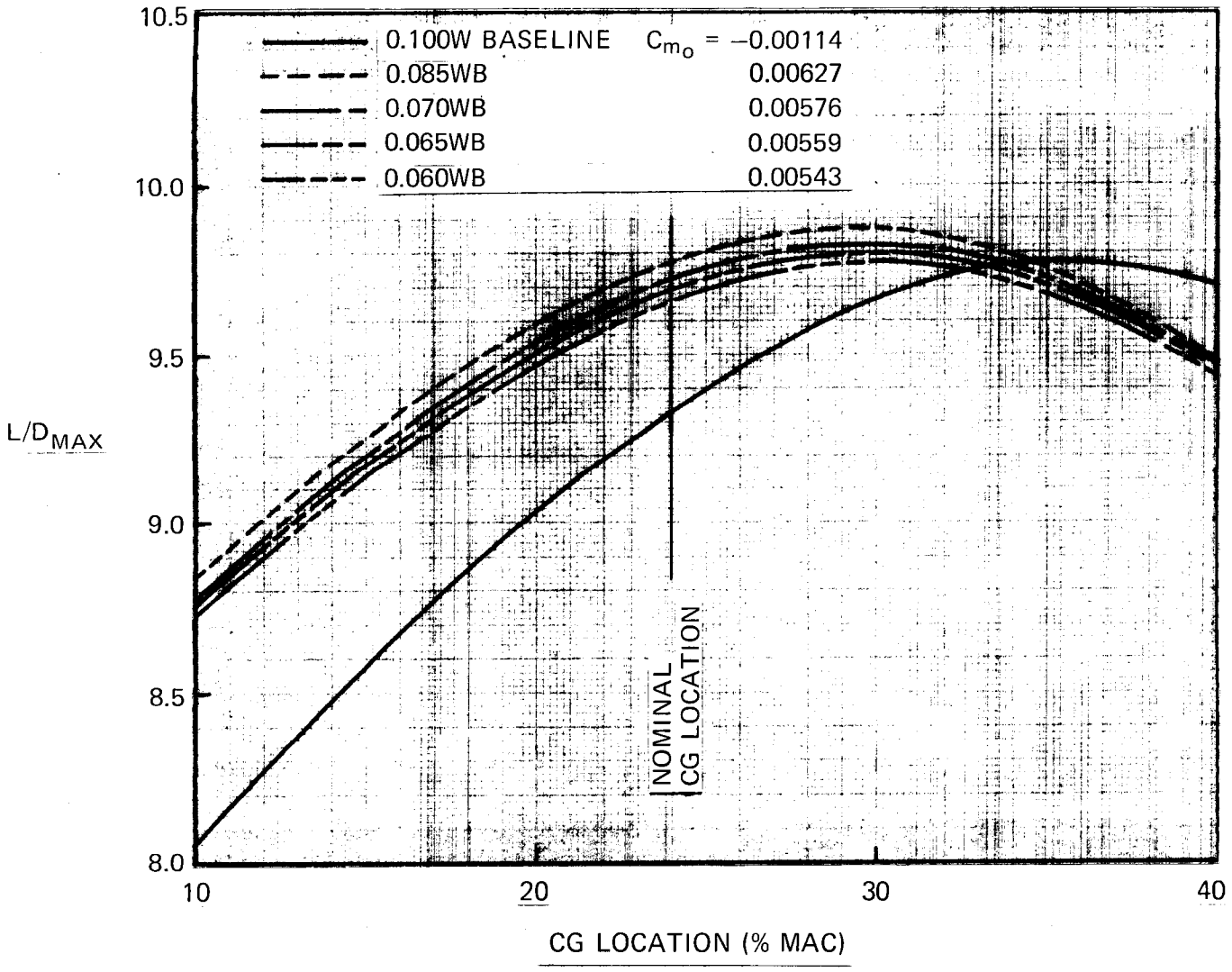

Figure 25. Effect of Wings Optimized in the Presence of a Fuselage at Low C_L's on L/D_{max} vs Center-of-Gravity Location

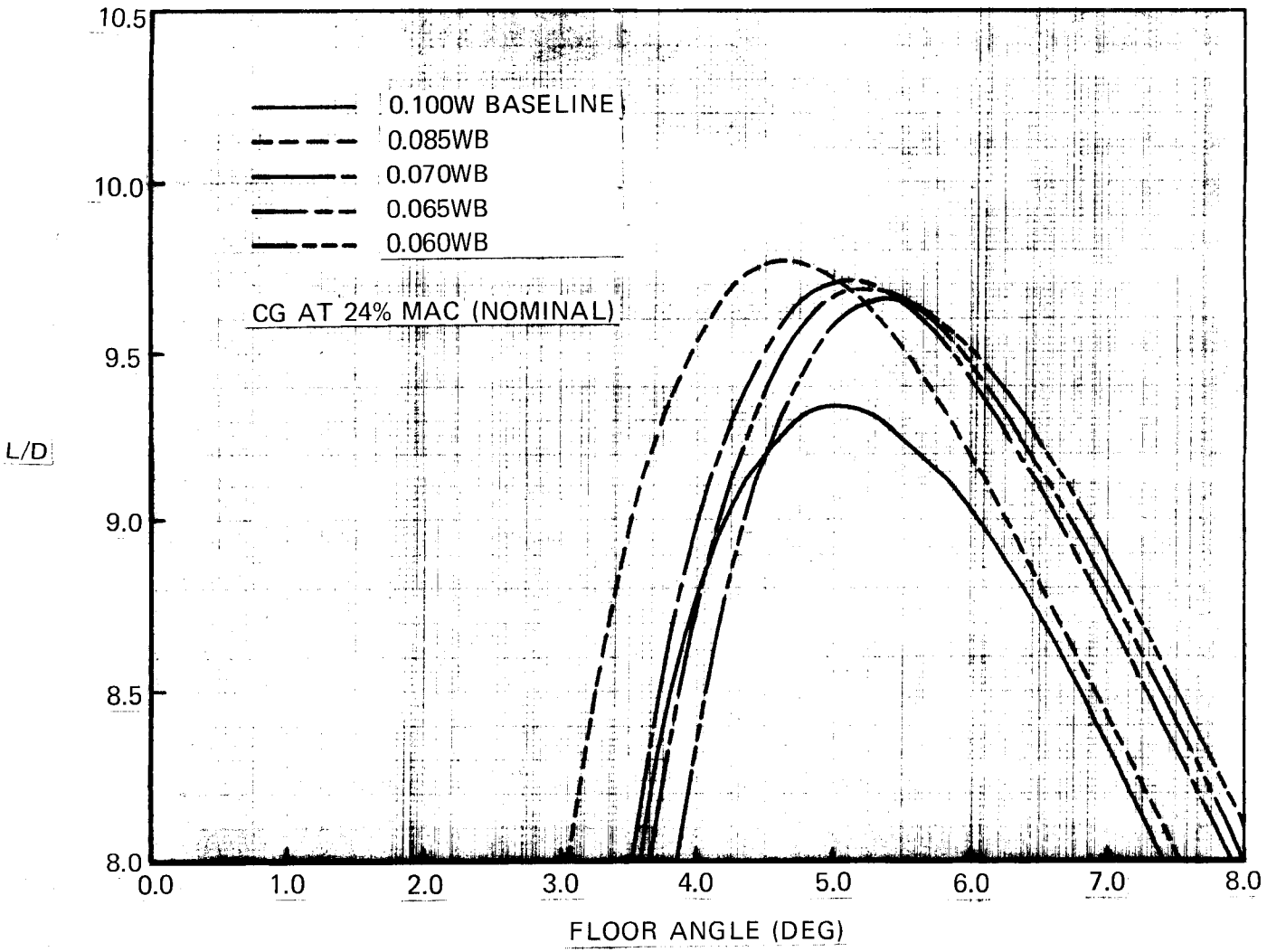

Figure 26. Effect of Wings Optimized in the Presence of a Fuselage at Low C_L's on L/D vs Floor Angle for the cg at 24% MAC (Nominal)

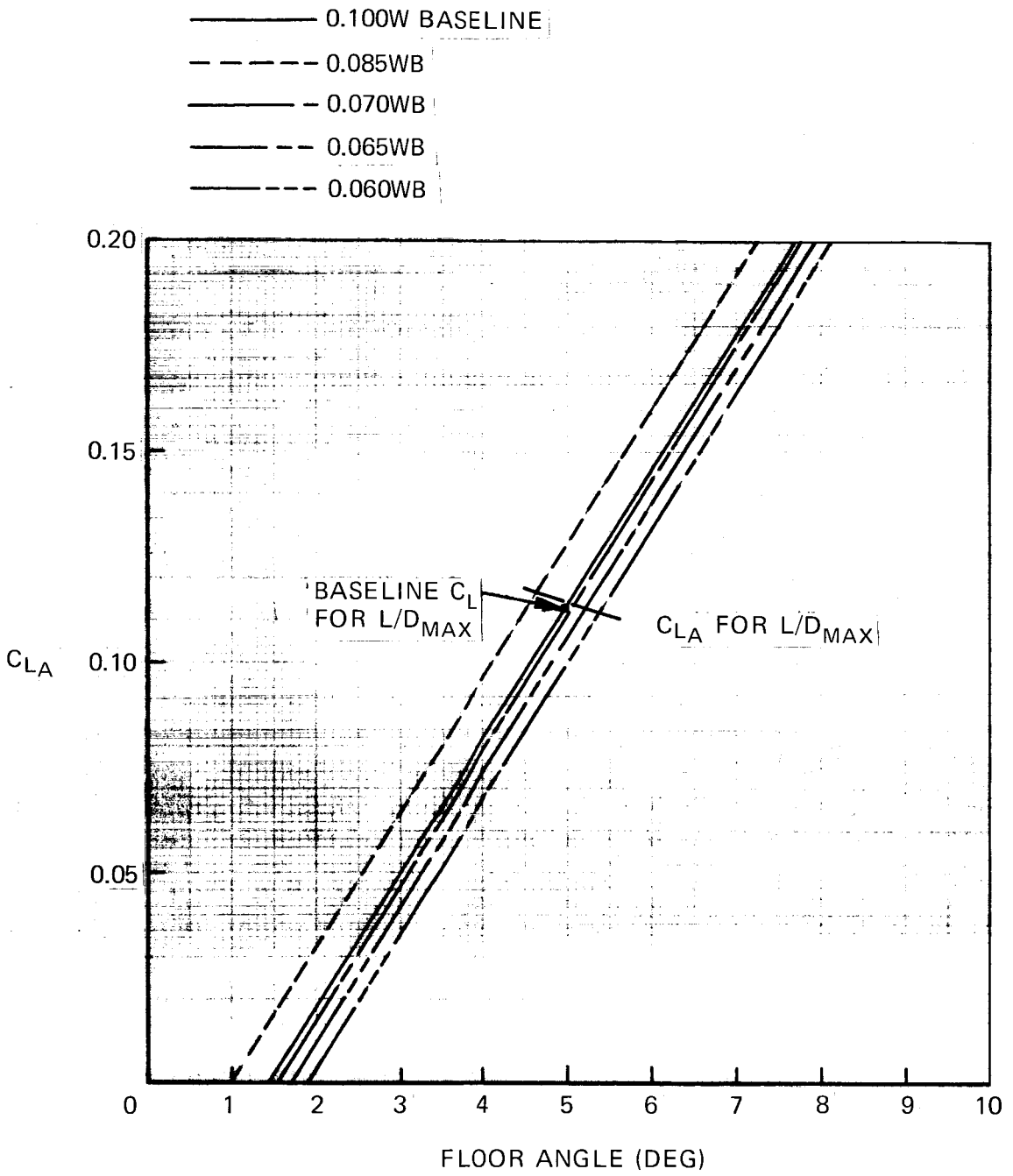

Figure 27. Lift Coefficient vs Floor Angle for Wings Optimized in the Presence of a Fuselage at Low C_L's

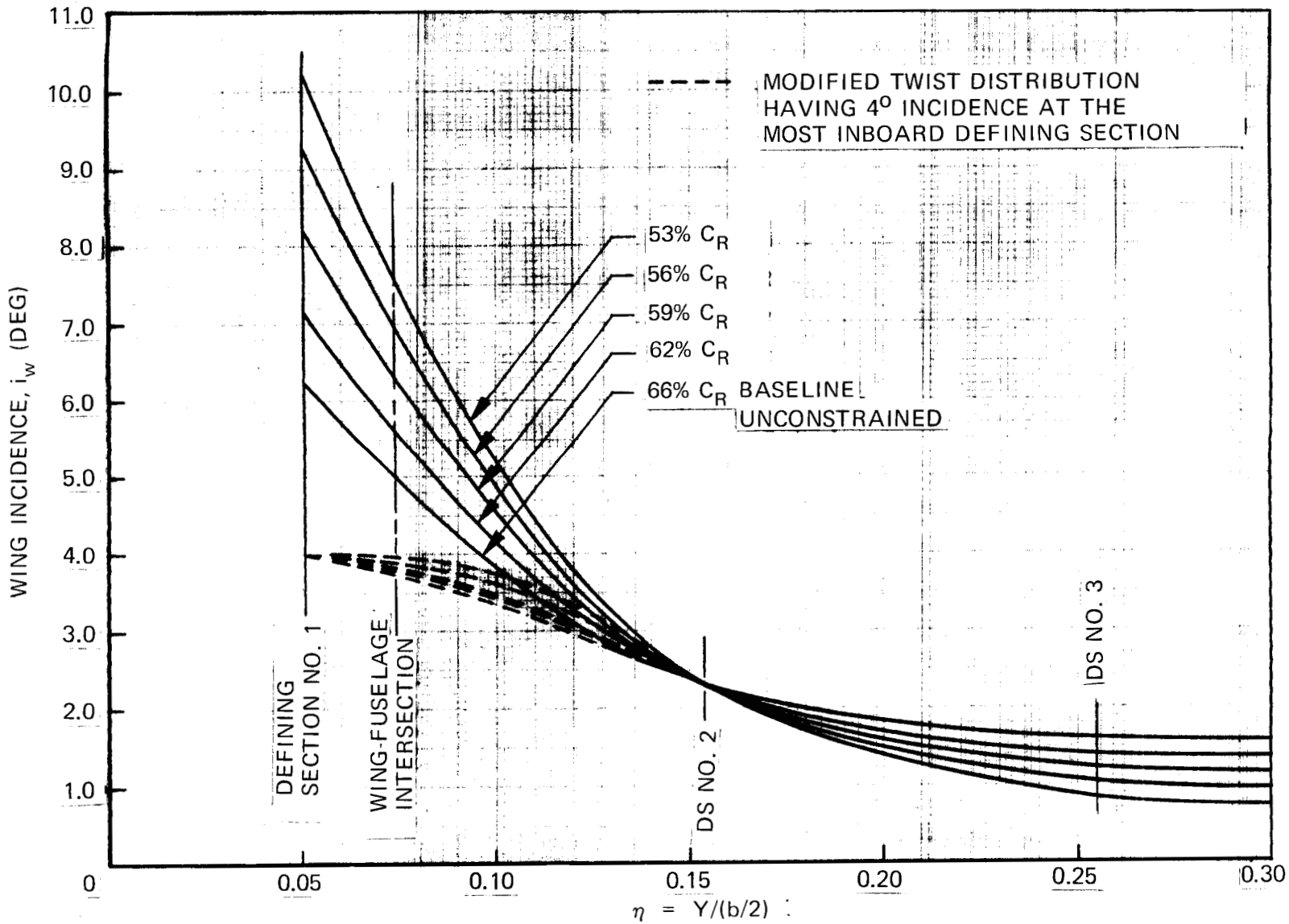

Figure 28. Inboard Wing Incidence for Wings Optimized With C_m Constraints

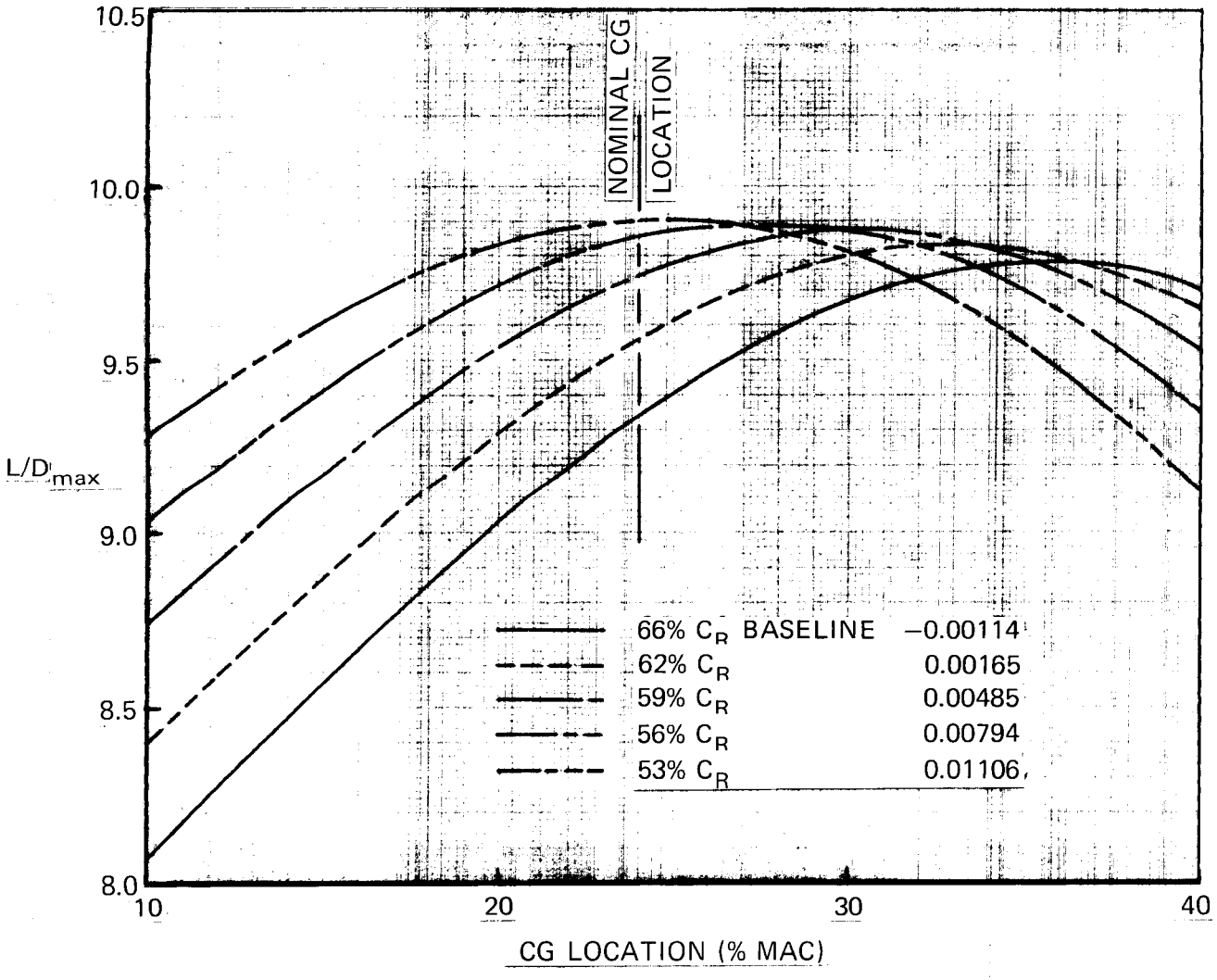

Figure 29. Effect of C_m Constrained Wings on L/D_{max} vs cg Location

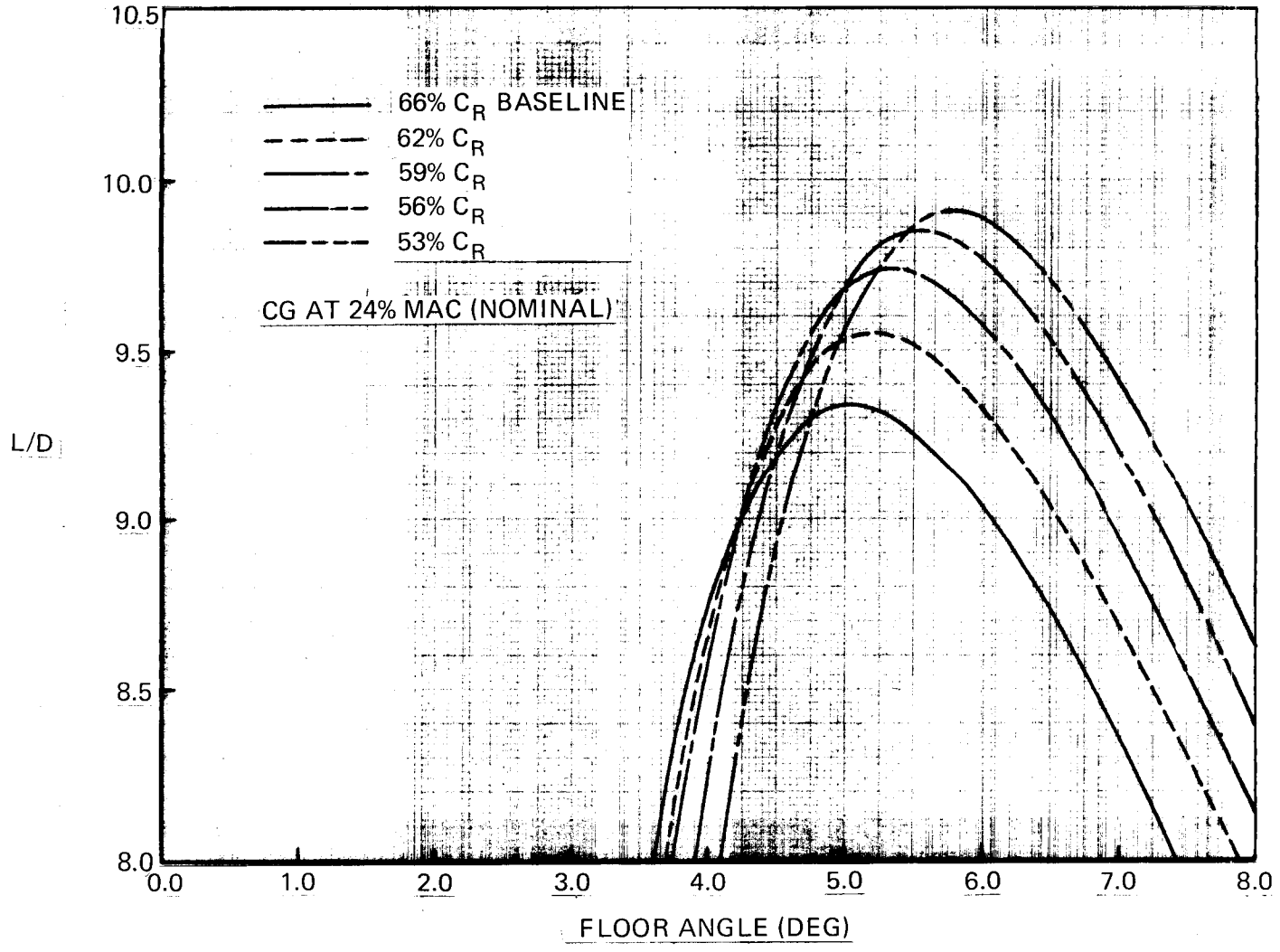

Figure 30. Effect of C_m Constrained Wings on L/D vs Floor Angle for the cg at 24% MAC (Nominal)

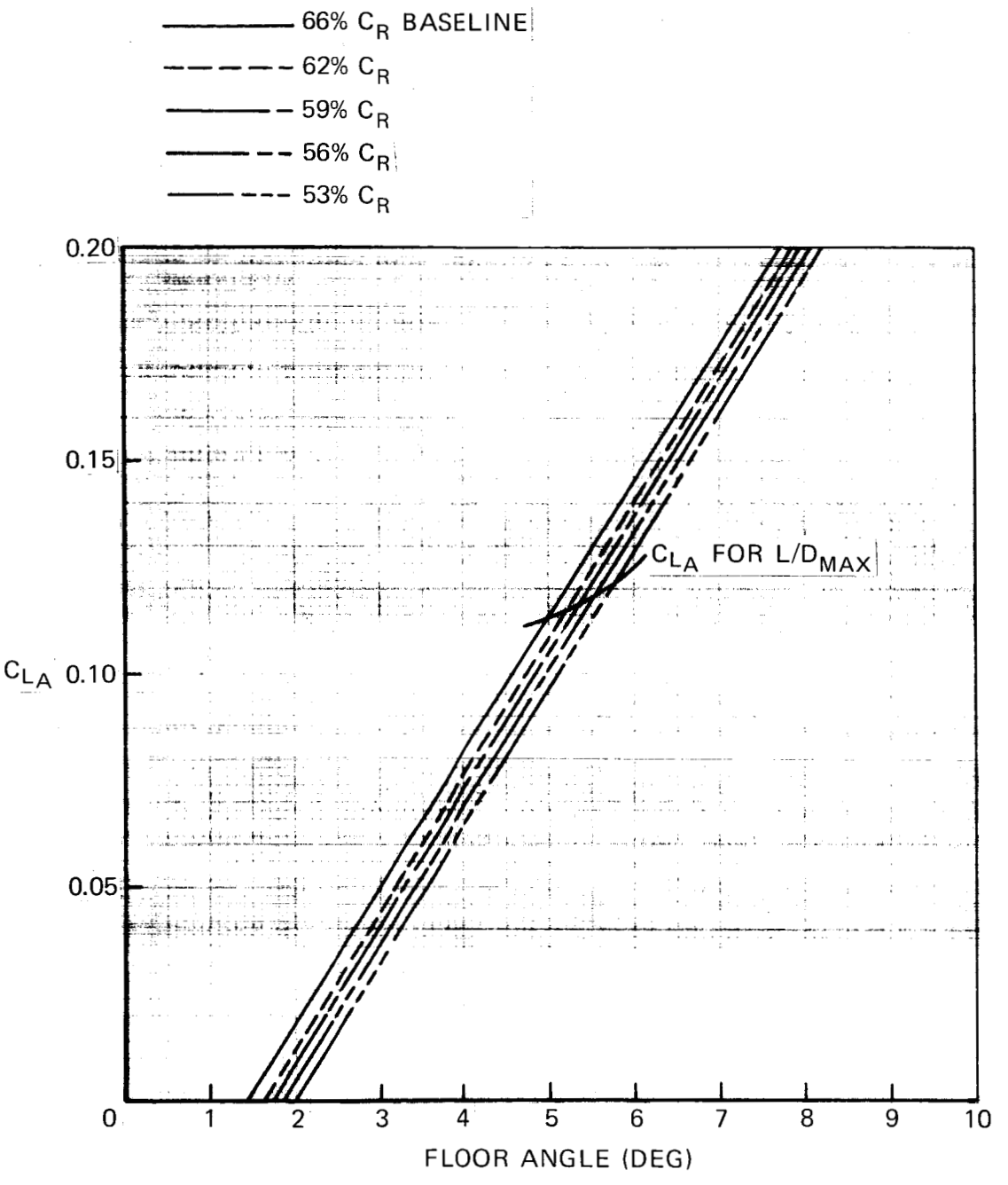

Figure 31. Lift Coefficient vs Floor Angle for Wings Optimized With C_m Constraints

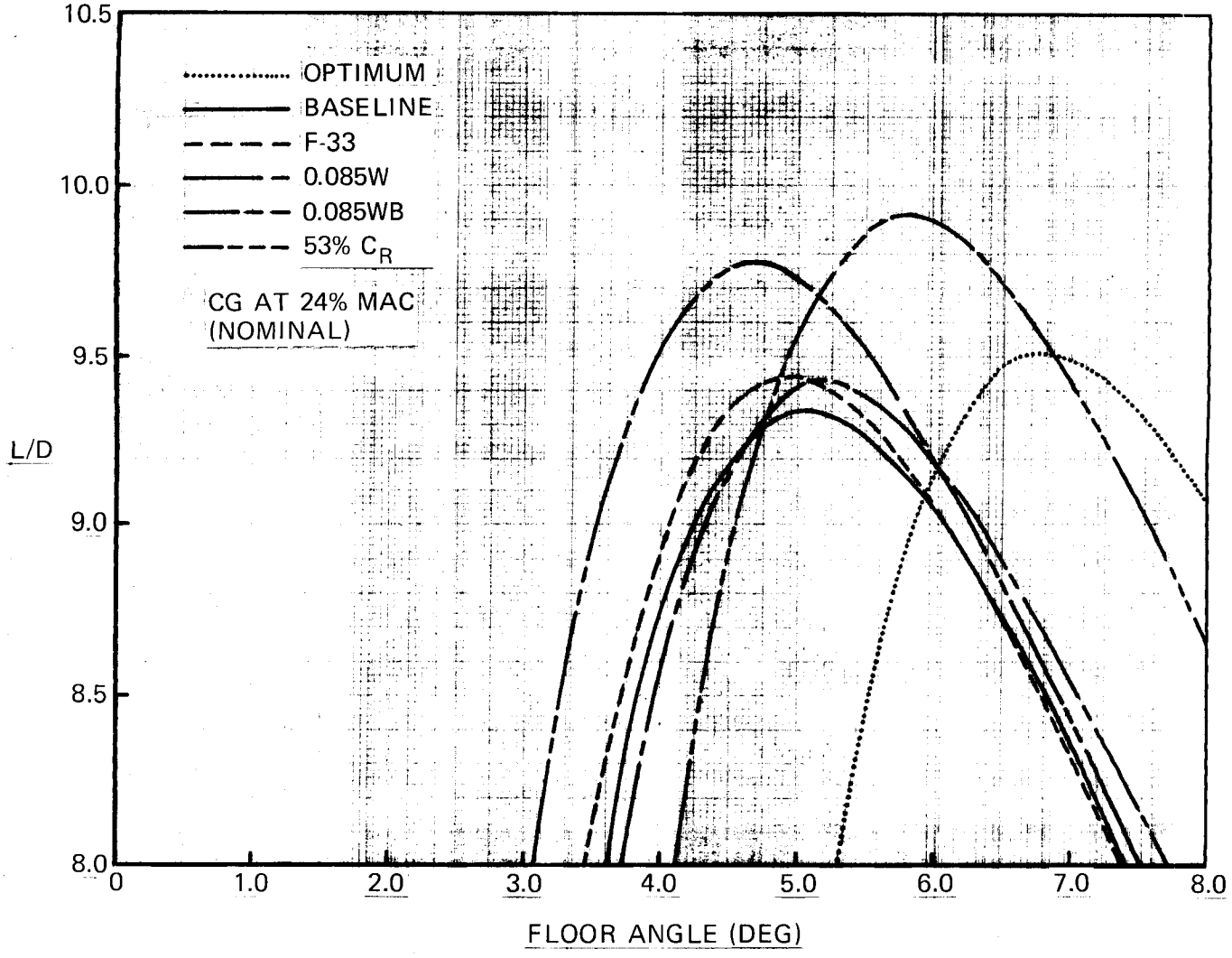

Figure 32. Comparison of L/D vs Floor Angle for the Best Configuration Resulting from Each Study

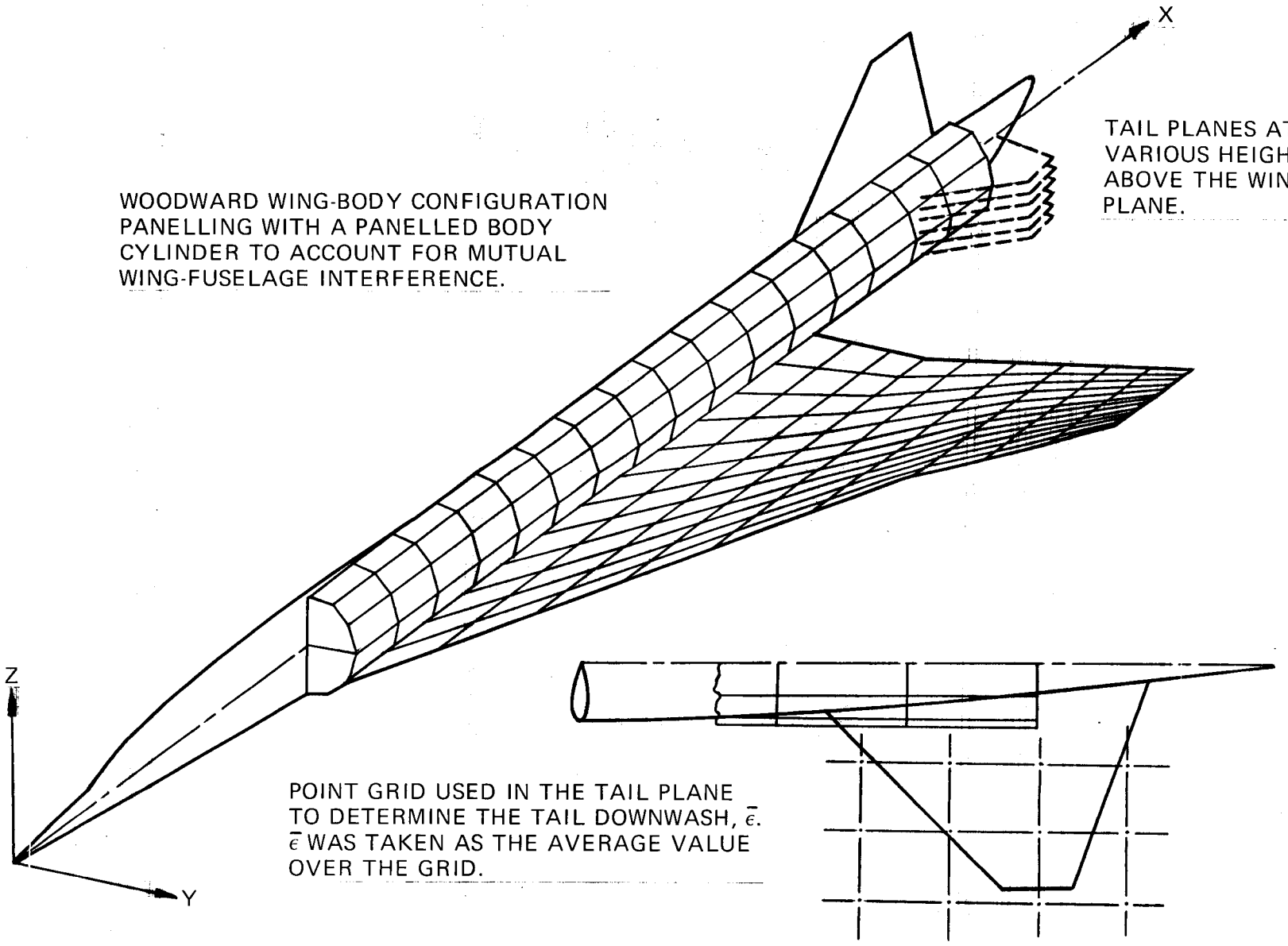

Figure 33. Depiction of Flow Visualization Grid Used for Horizontal Tail Downwash Survey

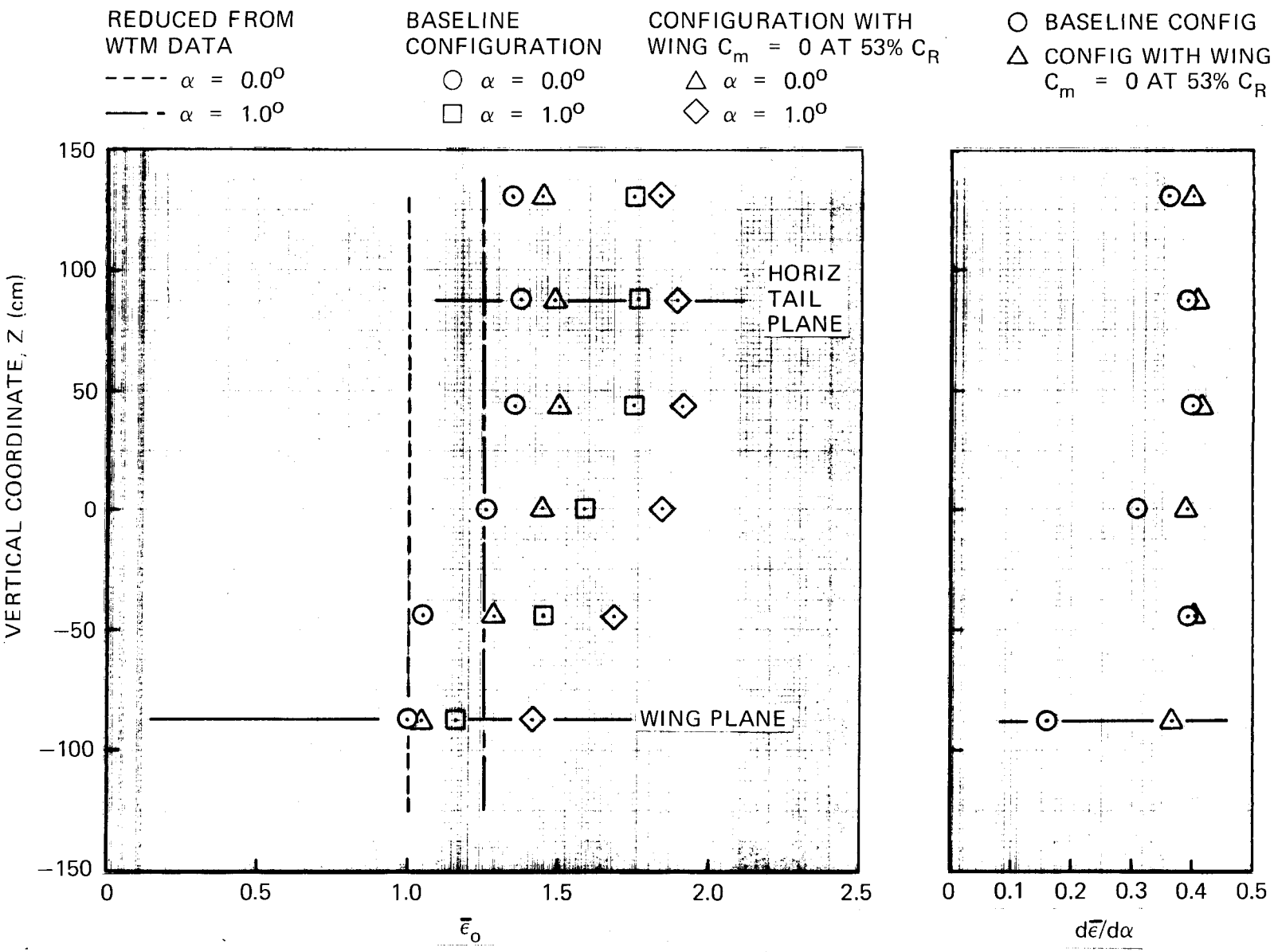

Figure 34. Average Downwash at the Tail at Various Heights Above the Wing Plane

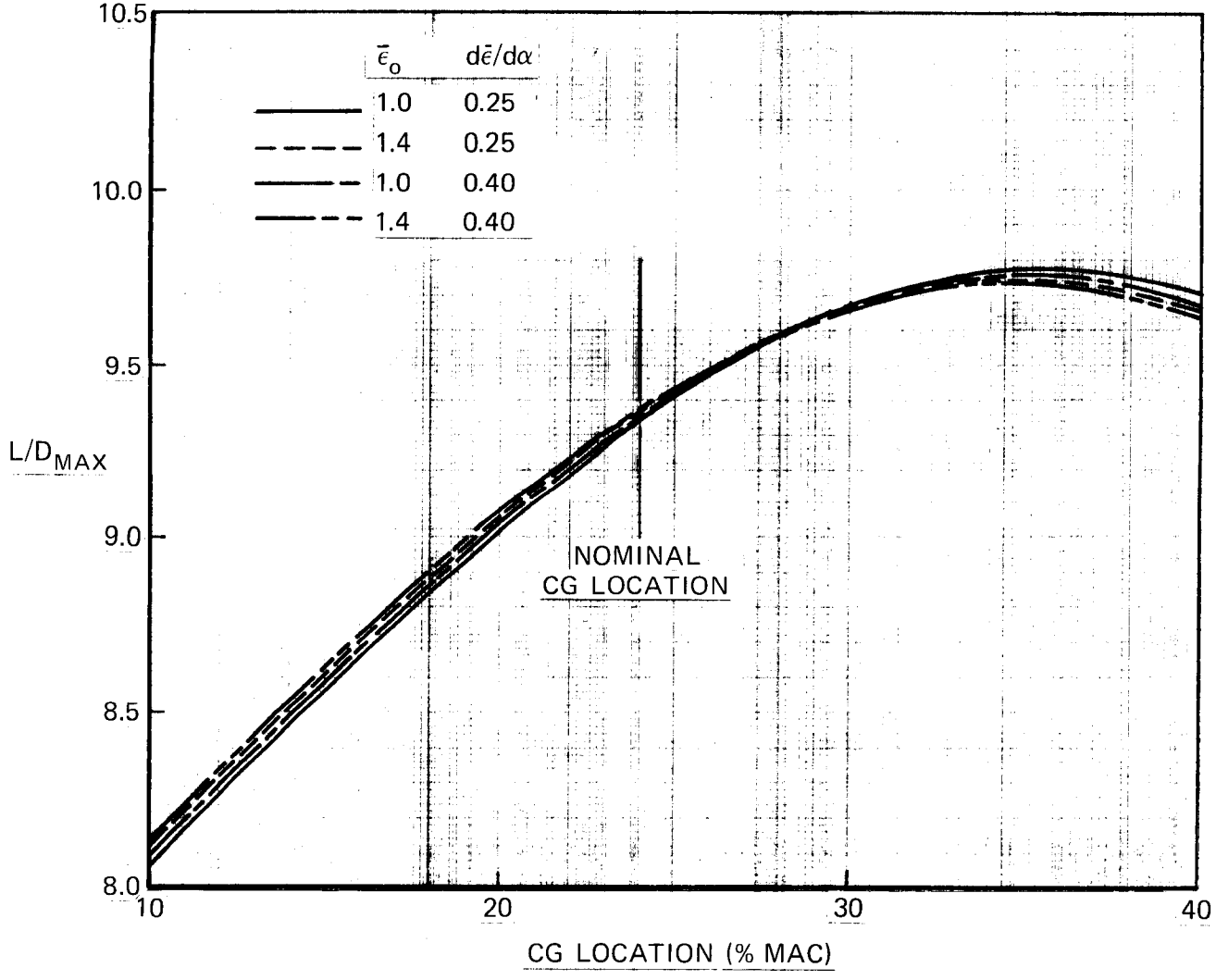

Figure 35. Effect of Variation of Downwash at the Horizontal Tail on L/D_{max} vs Center-of-Gravity Location for the Baseline Configuration